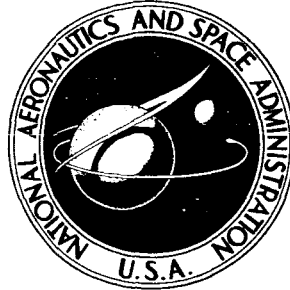


UNCLASSIFIED

~~CONFIDENTIAL~~



**NASA TECHNICAL  
MEMORANDUM**



NASA TM X-998

C2

CLASSIFICATION CHANGED

UNCLASSIFIED

To .....

By authority of *STAL* Date *12-31-70*  
*V.8 No. 24* / *blow*

*3-16-71*

**LIBRARY COPY**

SEP 2 1964

LANGLEY RESEARCH CENTER  
LIBRARY, NASA  
LANGLEY STATION  
HAMPTON, VIRGINIA

**INVESTIGATION OF THE HEAT TRANSFER  
TO THE HL-10 MANNED LIFTING  
ENTRY VEHICLE AT A MACH NUMBER OF 8**

*by James C. Dunavant and Philip E. Everhart*

*Langley Research Center*

*Langley Station, Hampton, Va.*

NATIONAL AERONAUTICS AND SPACE ADMINISTRATION • WASHINGTON, D. C. • AUGUST 1964

UNCLASSIFIED  
~~CONFIDENTIAL~~

UNCLASSIFIED  
~~CONFIDENTIAL~~

CLASSIFICATION CHANGED

To UNCLASSIFIED

By authority of STAR Date 12-31-70  
V. 8 No. 24 Blm  
3-16-71

INVESTIGATION OF THE HEAT TRANSFER TO THE

HL-10 MANNED LIFTING ENTRY VEHICLE

AT A MACH NUMBER OF 8

By James C. Dunavant and Philip E. Everhart

Langley Research Center  
Langley Station, Hampton, Va.

GROUP 4

Downgraded at 3 year intervals;  
declassified after 12 years

CLASSIFIED DOCUMENT—TITLE UNCLASSIFIED

This material contains information affecting the national defense of the United States within the meaning of the espionage laws, Title 18, U.S.C., Secs. 793 and 794, the transmission or revelation of which in any manner to an unauthorized person is prohibited by law.

NATIONAL AERONAUTICS AND SPACE ADMINISTRATION

UNCLASSIFIED

~~CONFIDENTIAL~~

UNCLASSIFIED

~~CONFIDENTIAL~~

INVESTIGATION OF THE HEAT TRANSFER TO THE

HL-10 MANNED LIFTING ENTRY VEHICLE

AT A MACH NUMBER OF 8\*

By James C. Dunavant and Philip E. Everhart  
Langley Research Center

SUMMARY

An experimental investigation of a reentry configuration having a hypersonic lift-drag ratio of about 1.0 has been conducted to determine the aerodynamic heating characteristics over the range of angle of attack from  $20^\circ$  to  $60^\circ$  which includes maximum lift-drag ratio and maximum lift coefficient. Measurements of heat transfer are compared with theoretical heating rates for swept infinite cylinders of arbitrary cross section. Along the curved lower-surface center line measured heat transfer and theory agree. Isolated cylinder theory predicted heating on the leading edge that was from 20 percent to 50 percent greater than the measured heating. The discrepancy is largest when the calculated stagnation point is closest to the tangency point of the leading edge and bottom surface. Deflecting the trailing-edge elevons downward  $30^\circ$  in some cases produced heating rates on the elevons as high as at the nose stagnation point.

INTRODUCTION

Studies of reentry at circular and supercircular velocities have shown the advantages of lifting reentry to achieve low maximum deceleration, lateral ranging capability, and low heating rates at the expense of higher heat loads. These studies have encompassed the range of hypersonic lift-drag ratio from about 0.5 to 2.0. One such study (ref. 1) has indicated that a vehicle having a hypersonic lift-drag ratio of about 1 should be considered to satisfy the possible requirements of a future reentry vehicle. Therefore, a study of the problems and the probable solutions associated with such an entry vehicle was undertaken at Langley Research Center. From this study has evolved the vehicle designated HL-10.

The concepts that led to the shape of the vehicle and some of the hypersonic aerodynamic characteristics of an early version of the HL-10 are presented in reference 2. Aerodynamic investigations of finned configurations are reported in references 3 and 4.

---

\*Title, Unclassified.

~~CONFIDENTIAL~~

UNCLASSIFIED

UNCLASSIFIED

~~CONFIDENTIAL~~

To obtain detailed heat-transfer distributions around the HL-10, an experimental investigation of the laminar heating characteristics was undertaken and the results are described herein. A calorimeter model of the HL-10 (with center dorsal fin E and tip fins D as defined in ref. 4) was tested in the Langley Mach 8 variable density tunnel at Reynolds numbers (based on model root chord) of  $0.24 \times 10^6$  to  $2.70 \times 10^6$ . The tests were made at angles of attack from  $20^\circ$  to  $60^\circ$  and with elevons at deflection angles of  $0^\circ$ ,  $30^\circ$ , and  $-60^\circ$ .

The complicated shape of the HL-10 largely prevents application of heat-transfer theories for simple shapes to the calculation of heating rates to the HL-10. However, the data have been compared with a theory for infinite cylinders of arbitrary cross section in order to determine the ability of such a theory to predict the level and distribution of heating to a blended wing-body combination.

#### SYMBOLS

c	chord
$c_w$	specific heat of wall material
$D_n$	nose diameter
h	heat-transfer coefficient
$h_o$	calculated stagnation-point heat-transfer coefficient on sphere of nose radius
K	thermal conductivity
m	weight of skin per unit heated surface area
M	Mach number
$N_{Pr}$	Prandtl number
p	pressure
r	radius
$R_c$	free-stream Reynolds number based on a root chord of 8 inches
s	surface distance from plane of symmetry
t	time

~~CONFIDENTIAL~~

UNCLASSIFIED

~~CONFIDENTIAL~~  
**UNCLASSIFIED**

T absolute temperature  
u velocity  
x,y,z model coordinates (see fig. 1)  
 $\alpha$  angle of attack (see fig. 1)  
 $\delta_e$  elevon deflection angle in plane normal to hinge line, positive with trailing edge down  
 $\mu$  dynamic viscosity  
 $\rho$  density

Subscripts:

e elevon  
t total  
2 condition behind normal shock  
w wall  
aw adiabatic wall  
 $\infty$  free stream  
 $\sigma$  static conditions just behind normal shock at free-stream Mach number

APPARATUS AND TESTS

Models

HL-10 configuration.- A drawing of the HL-10 configuration used for the heat-transfer model 8 inches long is shown in figure 1. The configuration tested is the version reported in reference 2 with a vertical fin (fin E of ref. 4) added at the center on top to provide directional stability and control at subsonic speeds and with canted tip fins (fin D of ref. 4) added to provide directional stability primarily at supersonic and hypersonic speeds. A table of body coordinates (the shape less tip fins and center fin) for the HL-10 heat-transfer model tested is given in table I.

The lower surface of the configuration is essentially a blunt-leading-edge delta wing with negative camber. The nose radius of the HL-10 is equal to the cylindrical leading-edge radius, although the leading edge is of constant radius for only about  $90^\circ$  of arc beginning on the lower surface. This leading-edge radius is faired into curves of larger radius which form the shape of upper surface. The lower surface is flat in the spanwise direction and has

~~CONFIDENTIAL~~  
**UNCLASSIFIED**

UNCLASSIFIED

~~CONFIDENTIAL~~

curvature only in the chordwise direction. The leading-edge radius of the tip fins is only one-third that of the nose and wing leading edge.

Model construction.- The thin-skin, calorimeter, heat-transfer model was made of 1/32-inch-thick inconel sheet formed over a mandrel in two halves, then welded together. Two photographs of the finished model are shown in figure 2. Both skin sections were attached with screws to the internal structure only at the edges of the cutout and around the elevons. The tip and center fin surfaces were separately formed and welded to the main portion of the body. Separate elevons were bent for the three elevon angles,  $0^\circ$ ,  $30^\circ$ , and  $-60^\circ$ , and were attached to the internal structure only at the forward edge of the elevon. Upper and lower surfaces of the elevon at  $0^\circ$  were made in one piece but the elevons deflected  $30^\circ$  and  $-60^\circ$  were split along a horizontal line at the center of the trailing edge of the elevon. Both upper and lower elevon surfaces were bent along their respective hinge lines to the desired deflection angle. The attachment of the upper surface cutout and the elevons can be seen in the photographs of the model in figure 2. All screw heads and small gaps at skin butt joints were filled in and carefully dressed off before the model was tested.

The mounting sting which was attached to the internal structure entered the model on the top near the rear and at an angle of  $30^\circ$  to the center line of the model (position of the sting is shown in figs. 1, 2, and 3). Strong interference effects on the flow over the upper surface in the vicinity of the elevons and center fin were produced. However, in view of the fact that the flow over the top surface is probably separated at these test angles of attack ( $20^\circ$  to  $60^\circ$ ) and the heat transfer is very low, it was decided to sacrifice the accuracy of the data in this area to obtain interference-free data on the lower surface.

A second model of fiber glass and resin was constructed of the HL-10 configuration with  $30^\circ$  elevon settings. This model was coated with a temperature-sensitive paint and tested at one tunnel condition. The color of the paint changed with temperature and, hence, for short exposure to the stream indicates approximately the relative degree of heating to the various parts of the model.

Model instrumentation.- The skin surface of the heat-transfer model was instrumented to measure heating rates by spot-welding No. 30 iron-constantan thermocouples to the inner surface at the locations shown in figure 3 and listed in table II. The thermocouples are largely laid out on the center line of the model and along five spanwise stations at  $x/c$  equal to 0.125, 0.250, 0.500, 0.750, and about 0.950. Skin thickness was measured at each thermocouple station and used in the data reduction. The thermocouple leads are contained in the sting except for the leads to the instrumented elevons which were taped to the outside of the sting.

#### Tests and Data Reduction

The model was tested in the Langley Mach 8 variable-density tunnel. Calibration data for the nozzle of this tunnel are given in reference 5. The stagnation conditions for the tests were pressures of approximately 65, 250, and

~~CONFIDENTIAL~~  
UNCLASSIFIED'

~~CONFIDENTIAL~~  
UNCLASSIFIED

1000 lb/sq in. abs and temperatures of about 800°, 900°, and 1000° F, respectively. The resulting test-section Mach numbers for these conditions are 7.59, 7.83, and 7.95, respectively, and the Reynolds numbers per foot are  $0.35 \times 10^6$ ,  $1.16 \times 10^6$ , and  $3.98 \times 10^6$ .

The heat-transfer data were obtained by means of a transient calorimeter technique. Steady-flow conditions are established in the test section with the model recessed in a chamber below the test section. The model and sting mount are then injected into the test section and pass through the tunnel-wall boundary layer in about 0.05 second.

The heat-transfer data were obtained by recording the temperature-time history of the model on magnetic tape with a digital data recorder. This system sampled the output of each thermocouple at the rate of 20 times per second and the data thus recorded were reduced to heat-transfer coefficients by the following equation:

$$h = \frac{mc_w}{(T_{aw} - T_w)} \frac{dT_w}{dt} \quad (1)$$

The weight of the material per unit surface area was corrected for surface curvature. The change in temperature with respect to time required in this equation was obtained by fitting a second degree polynomial by the method of least squares to a group of 21 data points obtained over a period of 1 second and differentiating this equation at the 11th point. The initial data point in the group falls between 1/4 and 1/2 second after the thermocouples first indicated an increase in the temperature of the skin. From continuous temperature-time traces (six selected thermocouple outputs were continuously monitored), it was determined that this period of time was sufficient to include the injection period during which the model was in the tunnel boundary layer and the portion of the temperature variation strongly affected by the finite conduction normal to the surface.

The adiabatic-wall temperature required in equation (1) was a calculated value for a laminar recovery factor and a Prandtl number of 0.7. The local temperature was determined by assuming that the flow expanded isentropically from the pressure behind a normal shock to the Newtonian pressure at the point in question. In the shadow region the pressure was assumed to be free-stream static pressure.

The heating rate was measured at 3/4 to 1 second after the initial temperature rise of the skin. During this period, in several of the tests, the model surface temperature rose as much as 150° F on the nose and on the surface of the elevon deflected downward 30°. In some areas, such as the one near the nose, the heating rate changes rapidly with distance along the surface and builds up large temperature gradients. The lateral surface temperature gradients that resulted in these tests were not large on the elevon but were enough in the region of the nose and the leading edge of the tip fins to cause significant lateral conduction of heat. Conduction estimates calculated for the worst conduction conditions of the tests show that the measured heating may be less than

~~CONFIDENTIAL~~

UNCLASSIFIED

the aerodynamic heating by as much as 10 percent at the stagnation point on the nose, 15 percent on the leading edge of the tip fins, and 5 percent on the leading edge of the body. No corrections for lateral conduction of heat have been applied to the data.

The measured heat-transfer coefficients are presented as the ratio  $h/h_0$  where  $h_0$  is the reference stagnation-point heat-transfer coefficient on a sphere having the same radius as the nose. The values were calculated for the particular test conditions from the following relation, which was adapted from reference 6:

$$h_0 = 0.763(N_{Pr})^{0.4} K_\sigma \left( \frac{\rho_\sigma}{\mu_\sigma} \frac{du}{ds} \right)^{0.5}$$

The stagnation-point velocity gradient is obtained from the modified Newtonian theory for the pressure distribution and is

$$\frac{du}{ds} = \frac{1}{r} \sqrt{\frac{2(p_{t,2} - p_\infty)}{\rho_{t,2}}}$$

The values of  $h_0$  calculated for the nominal test conditions are shown in the following table:

$P_t$ , lb/sq in. abs	$T$ , OF	$h_0$ , Btu/ft <sup>2</sup> -sec-OF	$R_c$
65	800	0.0111	$0.24 \times 10^6$
250	900	.0206	.77
1000	1000	.0403	2.70

These values of  $h_0$  are from 3 to  $4\frac{1}{2}$  percent greater than that which would be predicted by a modified form of the Fay and Riddell equation for the heat transfer to the stagnation point of a blunt body in a perfect gas. (This particular modification is given in ref. 7.) The measured and theoretical distributions of the heating ratio  $h/h_0$  shown herein are not expected to be invariant with Mach number or directly applicable to the higher flight Mach number region. However, the changes in distribution (exclusive of the elevons) that will occur at the higher flight Mach numbers are probably fairly small, and the results shown are believed to be representative of hypersonic flight for equilibrium boundary layers.

~~CONFIDENTIAL~~  
UNCLASSIFIED

## THEORY

To assess the predictability of the level of heating and distribution of heating, theoretical values were calculated for various portions of the model and are compared with the measured data at two representative angles of attack,  $30^\circ$  and  $50^\circ$ . Theory for a swept infinite cylinder of arbitrary cross section was used by considering the model divided into spanwise strips and calculating the heat transfer on the infinite cylinder of the same cross section as the body and on the tangent to the body. The longitudinal component of the flow was neglected in accordance with the sweepback principle, and streamline divergence was not taken into account. In addition, the heat transfer to the  $90^\circ$  segment of a cylinder forming the leading edge was calculated as though it were part of an isolated infinite swept cylinder.

### Stagnation-Line Distributions

An expression adapted by Bertram and Everhart (eq. (10) in ref. 7) from the Fay and Riddell relation for laminar stagnation-point heating was used to calculate the heating along the center line of the model and the stagnation line on the leading edge. This theory was applied to the present configuration by using the velocity gradient as given in reference 7. Also, the difference in shape of the model spanwise cross section at the leading edge from a circular segment was neglected.

### Spanwise Distribution of Heating

Spanwise distributions of heating were calculated as the ratio of local heat transfer to the stagnation-line heat transfer by applying the theory of Lees (ref. 8) to the blunt two-dimensional cross-sectional shape forming the body. In the case wherein the body was assumed to be divided into spanwise strips, the calculation was performed for the region from the stagnation line at the center of the model to the point on the edge of the cross section where the surface is normal to the surface at the center of the cross section. This theory is called the "cross-flow theory" and is presented as the ratio of the local heating to the reference stagnation-point heating  $h_0$ . The results obtained, with the  $90^\circ$  circular segment forming the leading edge assumed to be part of an isolated infinite swept cylinder, are called "isolated cylinder theory." The pressure distribution required to obtain these results from Lees theory was taken from the data correlation and extrapolation of reference 9. The data given in reference 9 are pressures for three-dimensional flow on disks of varying edge radii normal to the flow. The stagnation-point velocity gradient obtained from reference 9 was subsequently revised and presented in reference 7. This revised and more accurate stagnation-point velocity gradient was used in calculating the stagnation-line heating but it was necessary to use the unrevised data of reference 9 for the spanwise pressure distributions.

~~CONFIDENTIAL~~

UNCLASSIFIED

~~CONFIDENTIAL~~  
UNCLASSIFIED

## DISCUSSION OF RESULTS

### Distribution of Heating Along Center Line

The ratio of the measured heat-transfer coefficient to the calculated stagnation-point heat-transfer coefficient is presented in figure 4 for the angles of attack and unit Reynolds numbers tested. The negative values of  $x/c$  are used to represent the heating on the top center line of the model. Representative side-view schlieren photographs taken during the tests with the undeflected elevons are shown in figure 5, and with the deflected elevons in figure 6. The lower surface near the nose of the HL-10 is seen to be nearly normal to the flow at the higher test angles of attack. High pressures which existed in this region along with the small local span of the forward portion are the apparent causes for the high heat transfer measured in this region. The effect of increasing the stream Reynolds number by a factor of about 10 in the tests is to decrease the heating ratio by about 20 percent. (See figs. 4(a) and 4(c).) The chordwise distributions of  $h/h_0$  are similar at the three Reynolds numbers except for the two rearmost ratios at the highest angle of attack in figure 4(c). This apparent rise in the heating ratio above that of the lower Reynolds numbers could be the beginning of transition but the data obtained here are insufficient to allow the cause to be determined with certainty. The theoretical results for the center line compared with the data in figure 4 show good agreement. Some of this agreement is probably fortuitous, for the theory is used over a local angle of attack ranging from about  $15^\circ$  to  $70^\circ$ , probably beyond its range of usefulness. However, from this agreement, it appears that the principal effect that the lower-surface curvature has on the heat transfer is a result of local angle of attack.

### Spanwise Distributions of Heating

The measured spanwise distributions of heating at the five chordwise measuring stations,  $x/c = 0.125, 0.250, 0.500, 0.750$ , and about  $0.950$  are presented in figures 7 to 11, respectively. Parts (a), (b), and (c) of each figure are for Reynolds numbers (based on the root chord) of  $0.24 \times 10^6$ ,  $0.77 \times 10^6$ , and  $2.70 \times 10^6$ , respectively. The distributions plotted begin on the lower center line and extend, at  $x/c = 0.125$ , all the way around to the top center line. At  $x/c = 0.250, 0.500$ , and  $0.750$  the distributions extend around the  $90^\circ$  arc leading-edge section and well up onto the relatively flat "side" of the vehicle. (See the respective cross sections in fig. 3.) The distribution at  $x/c \approx 0.950$  includes the thermocouples located on the lower elevon surface and also extends around the tip fin including in this distribution a thermocouple on the leading edge of the tip fin and one on the inner surface of the tip fin. Generally, the small trend of decreasing  $h/h_0$  with increasing stream Reynolds number found at the center line is the same for the spanwise distributions when the elevon is not deflected.

The shapes of the cross sections at the various stations are formed by a flat section (in the spanwise direction) at the center and a leading edge of circular cross section in a plane normal to the leading edge. The leading edge

~~CONFIDENTIAL~~  
UNCLASSIFIED

UNCLASSIFIED

is so nearly circular in the plane normal to the chord that this small difference is disregarded. The constant leading-edge radius with the changing span from nose to trailing edge forms dissimilar spanwise cross sections. Some effects of these dissimilar cross sections and the varying span dimension are evident in the measured heat transfer. At  $x/c = 0.125$  and  $0.250$  (figs. 7 and 8) the heating on the center at high angles of attack is nearly as great as the peak heating which occurs on the leading edge, whereas at a typical rearward station,  $x/c = 0.750$  (fig. 10), the peak heating on the leading edge is frequently two to three times the heating at the center of the wing lower surface.

The cross-flow theory and the isolated cylinder theory for the  $\alpha = 30^\circ$  and  $\alpha = 50^\circ$  conditions are compared with the measured data in figures 7 to 10. The cross-flow theory predicts no peak in the heating at the leading edge for the forwardmost station,  $x/c = 0.125$  (fig. 7), and only a small peak at the rearward station,  $x/c = 0.750$  (fig. 10). Much higher heating rates on the leading edge are predicted by the isolated cylinder theory for all chordwise stations. Maximum values predicted by the two theories are nearly equal at the forward chordwise station shown in figure 7, but at the rear station ( $x/c = 0.750$ ) the two theories differ by a factor of 3 or 4 (fig. 10). The data tend to fall between these two estimates in both heating level and distribution. At the forwardmost station,  $x/c = 0.125$  in figure 7, the measured values show a peak which is of lesser magnitude than that estimated by the isolated cylinder theory but more than that estimated by considering the entire cross section to be an isolated cylinder, as was done in the cross-flow theory. At the rearward station,  $x/c = 0.750$  in figure 10, the level of heating at the center of the model is accurately estimated by the cross-flow theory and the peak measured values on the leading edge are several times the center-line values. Furthermore, the cross-flow theory distributions on the wing show only a small increase around the leading edge. The isolated cylinder theory overestimates the heating. These results confirm previous statements that the simplified assumptions made for the flow field are the cause for the differences between the calculated and measured values shown in figures 7 to 10. In the case of the cross-flow theory, it was assumed that the component of the flow normal to the surface would determine the heat transfer. This assumption was seen to be adequate for the center line; however, this same component of flow could not be used in the region of the leading edge.

The isolated cylinder theory uses the component of flow normal to the leading edge; however, the theory was derived for a full cylinder isolated from other surfaces and swept at some angle to the flow. In the present study, this theory has been applied to a leading edge, which is only approximately a  $90^\circ$  segment of a cylinder, bounded on each edge by one flat and one nearly flat surface tangent to the cylinder surface. Furthermore, in some cases, the calculated stagnation line on the cylinder is located only about  $6^\circ$  of surface arc from the flat lower surface. This condition, which occurred at  $x/c = 0.250$  at  $\alpha = 50^\circ$  (see fig. 8) resulted in the largest difference (about 50 percent) between the isolated cylinder theory and the data. Where the stagnation line on the cylinder was calculated to be farther from the flat lower surface, the agreement between the isolated cylinder theory and the data is much better. Such a condition is shown in figure 10 where  $x/c = 0.750$  and  $\alpha = 30^\circ$ . Here the calculated stagnation line on the cylindrical portion of the leading edge

UNCLASSIFIED

UNCLASSIFIED

was located approximately  $44^\circ$  from the flat lower surface. For this condition the isolated cylinder theory overestimates the data by 19 to 22 percent.

### Heat Transfer to Deflected Elevons

Deflecting the elevons downward from the lower surface separates the flow over portions of the lower surface and produces some critically high heating rates on the elevon surfaces. The spanwise heat-transfer distribution at  $x/c \approx 0.950$ , which includes the heating to the elevon surfaces, is shown for the undeflected elevon in figure 11. The level of heating to the elevon surface is about the same as on the center line at this station but rises considerably toward the leading edge. The heat-transfer rates produced by deflecting the elevons  $30^\circ$  downward are plotted against the spanwise position in figure 12 and the chordwise position in figure 13. On the elevons the heating ratios are strongly dependent on Reynolds number; the highest heating ratios occur at the highest Reynolds numbers and the lowest at the lowest Reynolds numbers. As seen in figure 12(c), the heat transfer on the  $30^\circ$  elevon was, in some cases, as much as 15 percent greater than the stagnation-point heat transfer. These heating rates are the result of the separation of the flow from the lower surface and reattachment on the elevon with the resultant high heating rates.

A sketch of the results (fig. 14) of the test made on the fiber-glass model of the HL-10 coated with temperature-sensitive paint shows the distribution of heating more clearly than the calorimeter data in figure 12. This sketch (fig. 14) gives results for conditions approximately equal to those of the  $\alpha = 40^\circ$  test of figure 12(b). The model was exposed to the aerodynamic heating for 3 seconds by injecting and retracting the model. The surface areas having the higher heat transfer changed color from the original pink to blue (first color change) and then olive (second color change). Regions of lower heating changed only to blue and where the heating was very low the surface remained pink. A region of higher heating is observed to cross the elevons diagonally, near midchord of the elevon and this region is believed to be the reattachment area. Examination of the measured heat transfer in figure 12(b) or 13 for this same condition,  $\alpha = 40^\circ$ , shows that the chordwise point of maximum heating on the elevons is similarly located. This point of maximum heating moves toward the hinge line with increasing Reynolds number. The increase in the level of heating on the elevon with Reynolds number suggests that boundary-layer transition is occurring over the separated region and reattachment is changing from laminar to turbulent. The increased level of heating on the elevons with increased angle of attack is in about the same proportion as the increase in heat transfer that occurs at this station with the elevons not deflected.

The extent of the separation on the lower surface caused by the elevons being deflected downward can be seen by comparing the heat transfer at  $x/c = 0.750$  for the deflected and undeflected conditions, figures 15 and 10. Laminar separation is strongly suggested by the decrease in the heating rate which occurred when the elevon was deflected downward. By comparing figures 15 and 10, laminar separation is indicated in a region in the center of the lower surface at  $\alpha = 40^\circ$  with some indications at  $\alpha = 30^\circ$ . The span of the model is less at this station ( $x/c = 0.750$ ) than at the elevon station ( $x/c = 0.950$ )

UNCLASSIFIED

~~CONFIDENTIAL~~  
~~CONFIDENTIAL~~

but the laminar separation is apparently confined to a center region of considerably less span than that of the elevons. At the higher Reynolds number (fig. 15(b)), similar regions of separation are shown at all three angles of attack ( $20^\circ$ ,  $30^\circ$ , and  $40^\circ$ ). At the highest Reynolds number (fig. 15(c)) the heating at  $\alpha = 30^\circ$  indicates no laminar separation while at  $\alpha = 20^\circ$  and  $40^\circ$  there is evidence of some laminar separation at  $x/c = 0.750$ . There is no increase in the heat transfer to the lower surface which would indicate transition before separation. The chordwise distribution of heating along the center line of the model with the elevons deflected  $30^\circ$  is presented in figure 16 and shows that the laminar separated region does not extend much ahead of  $x/c = 0.625$ .

The heat transfer measured on the elevons when they are set at  $-60^\circ$  is shown in the spanwise distributions for  $x/c \approx 0.950$  plotted in figure 17. The heating, as would be expected at this condition, is low, 5 percent or less of the stagnation-point heating. Deflecting the elevons upward had no apparent effect on the heat transfer to other lower surface stations as is shown by comparing the heating of figure 18 which is the distribution at  $x/c = 0.750$  with the elevon deflected upward,  $-60^\circ$ , with the same conditions for the undeflected elevon, figure 10.

The heat transfer to the upper surface of the elevons was not large, usually less than about 2 percent of the stagnation-point heating. These quantities are given in table III as the ratio of the measured heat-transfer coefficient to the stagnation-point heat-transfer coefficient.

#### Heat Transfer to Tip Fins

The heat transfer to the leading edge of the tip fin is apparently not a great problem. The highest heat transfer measured on the tip-fin leading edge was about 40 percent of the stagnation-point heating rate at  $\alpha = 20^\circ$  (see fig. 11 or 12) and decreased at higher angles of attack. As mentioned previously, the tip-fin leading-edge heating rates are affected by lateral conduction; this effect was estimated to increase the heating rate by only about 15 percent. A further error may be caused by failure to locate the tip-fin leading-edge thermocouple exactly on the stagnation line.

Additional measurements made at stations on and around the tip fins are listed in table III (other than  $x/c \approx 0.950$  which is plotted). Locations of these measuring stations can be found in figure 3 and table II. Data for some other thermocouple locations, for instance a few locations on the upper surface, which are of less interest, are also given in table III.

#### CONCLUSIONS

A model of a manned lifting entry vehicle designated the HL-10 has been tested at a Mach number of 8 and at three Reynolds numbers from  $0.24 \times 10^6$  to  $2.70 \times 10^6$  with three elevon angles,  $0^\circ$ ,  $30^\circ$ , and  $-60^\circ$ . From measurements of the heat transfer to the configuration and comparison of these values with

~~CONFIDENTIAL~~  
~~CONFIDENTIAL~~  
UNCLASSIFIED

~~CONFIDENTIAL~~  
**UNCLASSIFIED**

theoretical heating rates for a swept infinite cylinder of arbitrary cross section, the following conclusions were obtained:

1. The heat transfer measured along the curved lower-surface center line is in agreement with that calculated for the tangent infinite cylinder of similar cross section for the range of local angles of attack from about  $15^{\circ}$  to  $70^{\circ}$ .
2. Considering the leading-edge segment to be an isolated cylinder results in a prediction of heating which was about 20 percent to 50 percent greater than the measured heating. The discrepancy is largest when the calculated stagnation point is closest to the tangency point of the leading edge and flat bottom surface.
3. Deflecting the elevons downward  $30^{\circ}$  causes laminar separation on the lower surface and reattachment heating rates on the elevons which vary greatly with Reynolds number. These heating rates may be greater than the stagnation-point heating on the nose at some test conditions.
4. Deflecting the elevons upward  $-60^{\circ}$  produced no change in heating to the lower surface of the body adjacent to the elevons. Heating rates of less than about 5 percent of the stagnation-point heating rate were measured on the elevon.
5. The maximum heat transfer to the leading edge of the tip fins at an angle of attack of  $20^{\circ}$  is probably not much more than 40 percent of the stagnation-point heating rate on the nose, and at higher angles of attack, the heating is much less.

Langley Research Center,  
National Aeronautics and Space Administration,  
Langley Station, Hampton, Va., March 31, 1964.

~~CONFIDENTIAL~~  
**UNCLASSIFIED**

UNCLASSIFIED

~~CONFIDENTIAL~~

#### REFERENCES

1. Love, E. S., and Pritchard, E. B.: A Look at Manned Entry at Circular to Hyperbolic Velocities. 2nd Manned Space Flight Meeting (Dallas, Texas), American Inst. Aero. and Astronautics, Apr. 1963, pp. 167-180.
2. Rainey, Robert W., and Ladson, Charles L.: Preliminary Aerodynamic Characteristics of a Manned Lifting Entry Vehicle at a Mach Number of 6.8. NASA TM X-844, 1963.
3. Ware, George M.: Aerodynamic Characteristics of Models of Two Thick  $74^\circ$  Delta Manned Lifting Entry Vehicles at Low-Subsonic Speeds. NASA TM X-914, 1964.
4. Ladson, Charles L.: Aerodynamic Characteristics of a Manned Lifting Entry Vehicle at a Mach Number of 6.8. NASA TM X-915, 1964.
5. Stainback, P. Calvin: Heat-Transfer Measurements at a Mach Number of 8 in the Vicinity of a  $90^\circ$  Interior Corner Aligned With the Free-Stream Velocity. NASA TN D-2417, 1964.
6. Crawford, Davis H., and McCauley, William D.: Investigation of the Laminar Aerodynamic Heat-Transfer Characteristics of a Hemisphere-Cylinder in the Langley 11-Inch Hypersonic Tunnel at a Mach Number of 6.8. NACA Rep. 1323, 1957. (Supersedes NACA TN 3706.)
7. Bertram, Mitchel H., and Everhart, Philip E.: An Experimental Study of the Pressure and Heat-Transfer Distribution on a  $70^\circ$  Sweep Slab Delta Wing in Hypersonic Flow. NASA TR R-153, 1963.
8. Lees, Lester: Laminar Heat Transfer Over Blunt-Nosed Bodies at Hypersonic Flight Speeds. Jet Propulsion, vol. 26, no. 4, Apr. 1956, pp. 259-269, 274.
9. Bertram, Mitchel H., Feller, William V., and Dunavant, James C.: Flow Fields, Pressure Distributions, and Heat Transfer for Delta Wings at Hypersonic Speeds. NASA TM X-316, 1960.

~~CONFIDENTIAL~~

UNCLASSIFIED

UNCLASSIFIED

TABLE I.- HL-10 MODEL COORDINATES

[All dimensions are in inches]

x = 1		x = 2		x = 3		x = 4		x = 5		x = 6		x = 7	
y	z	y	z	y	z	y	z	y	z	y	z	y	z
0	0.591	0	0.647	0	0.651	0	0.651	0	0.651	0	0.651	0	0.654
.125	.569	.125	.637	.125	.647	.125	.642	.125	.634	.125	.634	.125	.636
.250	.496	.250	.607	.250	.639	.250	.627	.250	.585	.250	.564	.250	.560
.375	.349	.375	.549	.375	.617	.375	.617	.375	.569	.375	.514	.375	.440
.500	.074	.500	.454	.500	.582	.500	.601	.500	.564	.500	.502	.500	.398
.526	0	.625	.312	.625	.529	.625	.574	.625	.554	.625	.500	.625	.398
.547	-.125	.750	.074	.750	.446	.750	.541	.750	.540	.750	.497	.750	.398
.557	-.250	.781	0	.875	.318	.875	.497	.875	.522	.875	.489	.875	.398
.559	-.339	.812	-.125	1.000	.111	1.000	.432	1.000	.496	1.000	.480	1.000	.398
0	-.719	.832	-.250	1.041	0	1.125	.329	1.125	.458	1.125	.469	1.125	.398
		.843	-.375	1.075	-.125	1.250	.168	1.250	.404	1.250	.454	1.250	.398
		.848	-.536	1.100	-.250	1.321	0	1.375	.331	1.375	.434	1.375	.398
		0	-.961	1.118	-.375	1.355	-.125	1.500	.216	1.500	.409	1.500	.398
				1.129	-.500	1.380	-.250	1.636	0	1.625	.371	1.625	.398
				1.135	-.626	1.399	-.375	1.670	-.125	1.750	.309	1.750	.398
				0	-1.062	1.411	-.500	1.692	-.250	1.875	.209	1.875	.398
						1.415	-.620	1.704	-.375	1.984	0	2.000	.398
						0	-1.025	1.707	-.449	1.997	-.125	2.125	.382
								0	-.860	0	-.632	2.250	.374
												2.287	0
												0	-.365

UNCLASSIFIED

UNCLASSIFIED

~~CONFIDENTIAL~~

TABLE II.- THERMOCOUPLE LOCATIONS

Number	$x/c$	$s/D_n$	$x_e/c_e$	Location
1	0	----	----	Center line, nose
2	.031	----	----	Center line, upper surface
3	.062	----	----	Center line, upper surface
4	.125	----	----	Center line, upper surface
5	.188	----	----	Center line, upper surface
6	.031	----	----	Center line, lower surface
7	.062	----	----	Center line, lower surface
8	.125	----	----	Center line, lower surface
9	.188	----	----	Center line, lower surface
10	.250	----	----	Center line, lower surface
11	.312	----	----	Center line, lower surface
12	.375	----	----	Center line, lower surface
13	.500	----	----	Center line, lower surface
14	.625	----	----	Center line, lower surface
15	.750	----	----	Center line, lower surface
16	.125	.266	----	Lower surface
17	.125	.528	----	Leading-edge surface
18	.125	.790	----	Leading-edge surface
19	.125	1.052	----	Upper surface
20	.125	1.520	----	Upper surface
21	.125	2.200	----	Upper surface
22	.250	.627	----	Lower surface
23	.250	.889	----	Leading-edge surface
24	.250	1.151	----	Leading-edge surface
25	.250	1.413	----	Upper surface
26	.250	1.800	----	Upper surface
27	.250	2.267	----	Upper surface
28	.500	.667	----	Lower surface
29	.500	1.373	----	Lower surface
30	.500	1.635	----	Leading-edge surface
31	.500	1.897	----	Leading-edge surface
32	.500	2.159	----	Upper surface
33	.500	2.600	----	Upper surface
34	.500	3.033	----	Upper surface
35	.750	.667	----	Lower surface
36	.750	1.333	----	Lower surface
37	.750	1.667	----	Lower surface
38	.750	2.160	----	Lower surface
39	.750	2.422	----	Leading-edge surface
40	.750	2.684	----	Leading-edge surface
41	.750	2.946	----	Upper surface
42	.750	3.333	----	Upper surface
43	.375	----	----	Center line, upper surface
44	.500	----	----	Upper surface
45	.562	----	----	Upper surface
46	.625	----	----	Upper surface
47	.687	----	----	Upper surface
48	1.000	----	----	Center line, lower surface
49	.969	----	----	Center line, lower surface
50	.938	----	----	Center line, lower surface
51	.938	2.890	----	Leading-edge surface
52	.938	3.220	----	Tip fin, outer surface
53	.938	3.720	----	Tip fin, outer surface
54	.938	4.900	----	Tip fin, inner surface
55	.875	----	----	Tip fin, outer surface
56	.875	----	----	Tip fin, outer surface
57	.875	----	----	Tip fin, leading edge
58	.938	4.300	----	Tip fin, leading edge
59	----	----	----	Center vertical tail
60	----	----	----	Center vertical tail
61	1.000	----	----	Tip fin, inner surface
62	1.000	----	----	Tip fin, leading edge
63	1.000	----	----	Tip fin, outer surface
64	----	1.267	0.230	Elevon, upper surface
65	----	1.267	.486	Elevon, upper surface
66	----	1.267	.744	Elevon, upper surface
67	----	1.867	.245	Elevon, upper surface
68	----	1.867	.497	Elevon, upper surface
69	----	1.867	.748	Elevon, upper surface
70	----	1.120	.270	Elevon, lower surface
71	----	1.120	.514	Elevon, lower surface
72	----	1.120	.757	Elevon, lower surface
73	----	1.573	.254	Elevon, lower surface
74	----	1.573	.502	Elevon, lower surface
75	----	1.573	.752	Elevon, lower surface
76	----	2.027	.241	Elevon, lower surface
77	----	2.027	.494	Elevon, lower surface
78	----	2.027	.747	Elevon, lower surface

~~CONFIDENTIAL~~

UNCLASSIFIED

TABLE III.- RATIO OF MEASURED HEAT TRANSFER TO STAGNATION-POINT HEAT TRANSFER

Re	α, deg	h/h <sub>o</sub> at thermocouple number -																				
		43	44	45	46	47	59	60	55	56	57	Tip fin, x/c = 0.875			Tip fin, x/c = 1.000			Top surface of eleveon				
		Top surface					Center tail	Tip fin, x/c = 0.875					Tip fin, x/c = 1.000									
δ <sub>e</sub> = 0°																						
0.24 × 10 <sup>6</sup>	20	0.020	0.006	0.004	0.004	0.004	0.004	0.017	0.020	0.093	0.175	0.359	0.010	0.313	0.197	0.005	0.005	0.007	---	0.001	0.003	
	30	0.019	0.005	0.002	0.003	0.006	0.008	0.010	0.156	0.197	0.254	0.011	0.241	0.240	0.005	0.006	0.005	---	0.003	0.006		
	40	0.016	0.007	0.005	0.007	0.003	0.005	0.006	0.200	0.179	0.153	0.014	0.147	0.272	0.003	0.003	0.000	---	0.004	0.007		
	50	0.016	0.009	0.007	0.002	0.004	0.003	0.006	0.240	0.173	0.105	0.023	0.116	0.306	0.001	0.001	0.001	---	0.001	0.001		
	60	0.020	0.011	0.012	0.011	0.012	0.009	0.012	0.277	0.173	0.087	0.047	0.118	0.341	0.013	0.006	0.008	---	0.012	0.075		
0.77 × 10 <sup>6</sup>	20	0.030	0.008	0.005	0.005	0.006	0.014	0.029	0.085	0.171	0.338	0.006	0.293	0.187	0.005	0.008	0.008	---	0.003	0.004		
	30	0.026	0.007	0.004	0.003	0.003	0.010	0.009	0.141	0.179	0.256	0.013	0.235	0.222	0.007	0.010	0.009	---	0.006	0.005		
	40	0.023	0.010	0.009	0.016	0.014	0.008	0.008	0.180	0.162	0.154	0.022	0.138	0.247	0.003	0.002	0.002	---	0.004	0.004		
	50	0.035	0.015	0.009	0.004	0.004	0.005	0.011	0.232	0.167	0.110	0.036	0.096	0.279	0.004	0.003	0.009	---	0.006	0.010		
	60	0.004	0.005	0.006	0.008	0.006	0.006	0.010	0.243	0.152	0.081	0.062	0.100	0.296	0.004	0.005	0.010	---	0.005	0.006		
2.70 × 10 <sup>6</sup>	20	0.040	0.013	0.010	0.006	0.007	0.013	0.056	0.079	0.167	0.298	0.005	0.266	0.183	0.003	0.005	0.006	---	0.003	0.004		
	30	0.028	0.007	0.006	0.010	0.008	0.008	0.015	0.132	0.172	0.252	0.009	0.230	0.211	0.005	0.006	0.006	---	0.006	0.007		
	40	0.030	0.014	0.009	0.011	0.010	0.009	0.012	0.174	0.151	0.150	0.025	0.137	0.234	0.008	0.007	0.006	---	0.007	0.006		
	50	0.038	0.024	0.018	0.010	0.014	0.008	0.016	0.155	0.096	0.070	0.090	0.476	0.010	0.006	0.016	---	0.008	0.010			
	60	0.010	0.008	0.008	0.010	0.009	0.010	0.018	0.258	0.149	0.080	0.096	0.097	0.328	0.008	0.012	0.018	---	0.010	0.012		
δ <sub>e</sub> = 30°																						
0.24 × 10 <sup>6</sup>	20	0.019	0.007	0.005	0.005	0.004	0.016	0.020	0.089	0.180	0.350	0.008	0.312	0.202	0.002	0.003	0.005	---	0.005	0.015		
	30	0.018	0.005	0.004	0.005	0.004	0.008	0.011	0.150	0.189	0.259	0.013	0.237	0.231	0.003	0.006	0.023	---	0.008	0.027		
	40	0.014	0.009	0.003	0.012	0.007	0.005	0.009	0.161	0.163	0.143	0.007	0.145	0.256	0.011	0.032	0.075	---	0.019	0.050		
	60																					
0.77 × 10 <sup>6</sup>	20	0.031	0.009	0.004	0.010	0.010	0.015	0.028	0.089	0.175	0.362	0.011	0.306	0.193	0.002	0.003	0.010	---	0.006	0.022		
	30	0.027	0.007	0.003	0.004	0.003	0.009	0.011	0.141	0.180	0.276	0.016	0.235	0.220	0.009	0.022	0.051	---	0.015	0.040		
	40	0.023	0.014	0.012	0.016	0.017	0.017	0.009	0.160	0.154	0.147	0.009	0.137	0.241	0.045	0.087	0.132	---	0.026	0.068		
	60																					
2.70 × 10 <sup>6</sup>	20	0.043	0.012	0.010	0.005	0.007	0.012	0.057	0.089	0.178	0.373	0.007	0.316	0.196	0.005	0.012	0.025	---	0.015	0.034		
	30	0.029	0.007	0.007	0.010	0.010	0.011	0.016	0.131	0.171	0.255	0.014	0.227	0.209	0.054	0.084	0.084	---	0.026	0.065		
	40	0.030	0.020	0.013	0.019	0.016	0.010	0.014	0.165	0.112	0.127	0.020	0.139	0.317	0.072	0.129	0.166	---	0.046	0.098		
	60																					
δ <sub>e</sub> = -60°																						
0.24 × 10 <sup>6</sup>	40	0.015	0.008	0.006	0.000	0.004	0.004	0.005	0.207	0.182	0.153	0.014	0.150	0.150	0.003	0.004	0.008	---	0.005	0.010		
	50	0.018	0.009	0.001	0.004	0.001	0.003	0.007	0.260	0.179	0.109	0.027	0.123	0.312	0.001	0.004	0.010	---	0.005	0.009		
	60	0.026	0.014	0.012	0.010	0.010	0.010	0.020	0.310	0.185	0.088	0.047	0.125	0.356	0.006	0.021	0.039	---	0.014	0.030		
	60																					
0.77 × 10 <sup>6</sup>	40	0.023	0.016	0.014	0.012	0.018	0.008	0.010	0.193	0.168	0.156	0.019	0.140	0.255	0.008	0.008	0.011	---	0.014	0.013		
	50	0.035	0.018	0.011	0.005	0.006	0.005	0.010	0.234	0.159	0.100	0.035	0.121	0.282	0.004	0.012	0.027	---	0.008	0.010		
	60	0.004	0.004	0.005	0.006	0.006	0.005	0.010	0.279	0.165	0.089	0.062	0.106	0.304	0.009	0.020	0.050	---	0.016	0.031		
	60																					
2.70 × 10 <sup>6</sup>	40	0.030	0.010	0.006	0.007	0.006	0.006	0.010	0.178	0.152	0.149	0.027	0.138	0.236	0.017	0.018	0.022	---	0.015	0.018		
	50	0.035	0.024	0.018	0.009	0.014	0.008	0.017	0.230	0.152	0.097	0.058	0.114	0.356	0.008	0.020	0.050	---	0.015	0.014		
	60	0.018	0.015	0.012	0.011	0.011	0.015	0.016	0.288	0.169	0.090	0.084	0.123	0.317	0.014	0.036	0.086	---	0.032	0.046		
	60																					

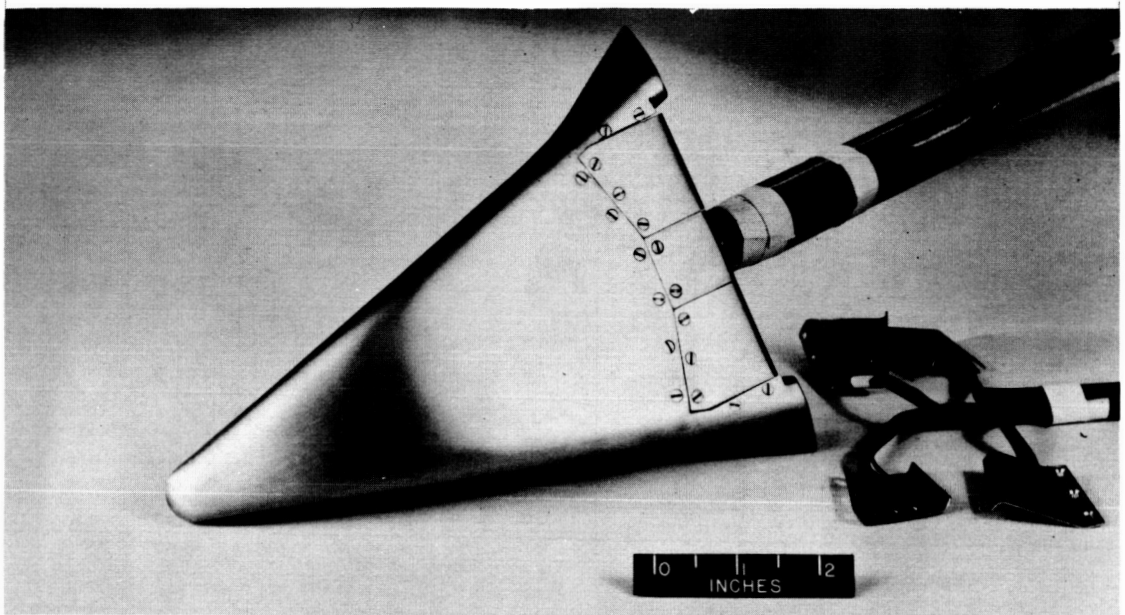
~~CONFIDENTIAL~~

The technical drawing illustrates the cross-sectional geometry of a ship's hull. It includes several key features and dimensions:

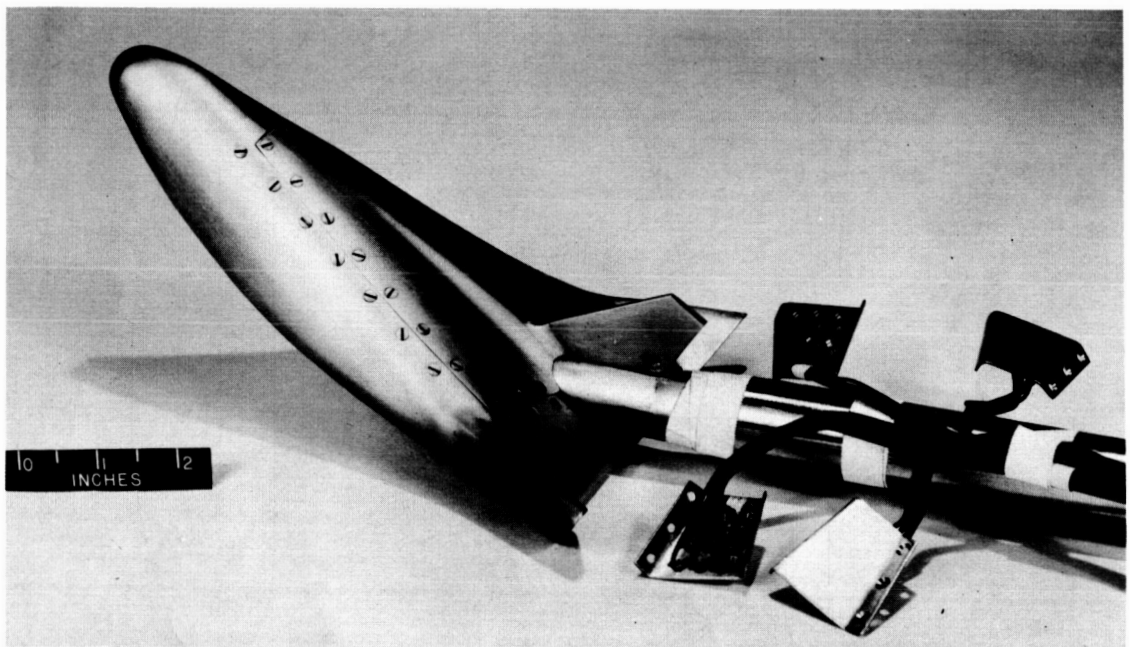
- Main Hull Dimensions:** The total width at the base is 8.000 units. The height from the baseline to the top of the main hull section is 1.137 units.
- Angles:** A large angle of  $16^\circ$  defines the lower part of the hull. Another angle of  $17^\circ$  is shown near the centerline.
- Internal Structure:** A central vertical section has a diameter of 0.500 units. The distance from the centerline to the inner edge of this section is 0.724 units.
- Handwritten Annotations:** In the upper right area, there are handwritten notes: "2 12.5° 60°", "-11.96", and "-15".
- Curvature and Radii:** Several radii are specified:  $0.375 \text{ rad}$ ,  $0.04 \text{ rad}$ ,  $0.004 \text{ rad}$ , and  $0.001 \text{ rad}$ .
- Other Dimensions:** Additional measurements include 1.55, 0.54, 0.667, 0.275, and 0.375.

Figure 1.- Model of Langley HL-10 configuration, with fins D and E. All dimensions are in inches.

UNCLASSIFIED



(a) Bottom view.



(b) Top view.

L-64-3055

Figure 2.- Photographs of HL-10 heat-transfer model.

UNCLASSIFIED

UNCLASSIFIED

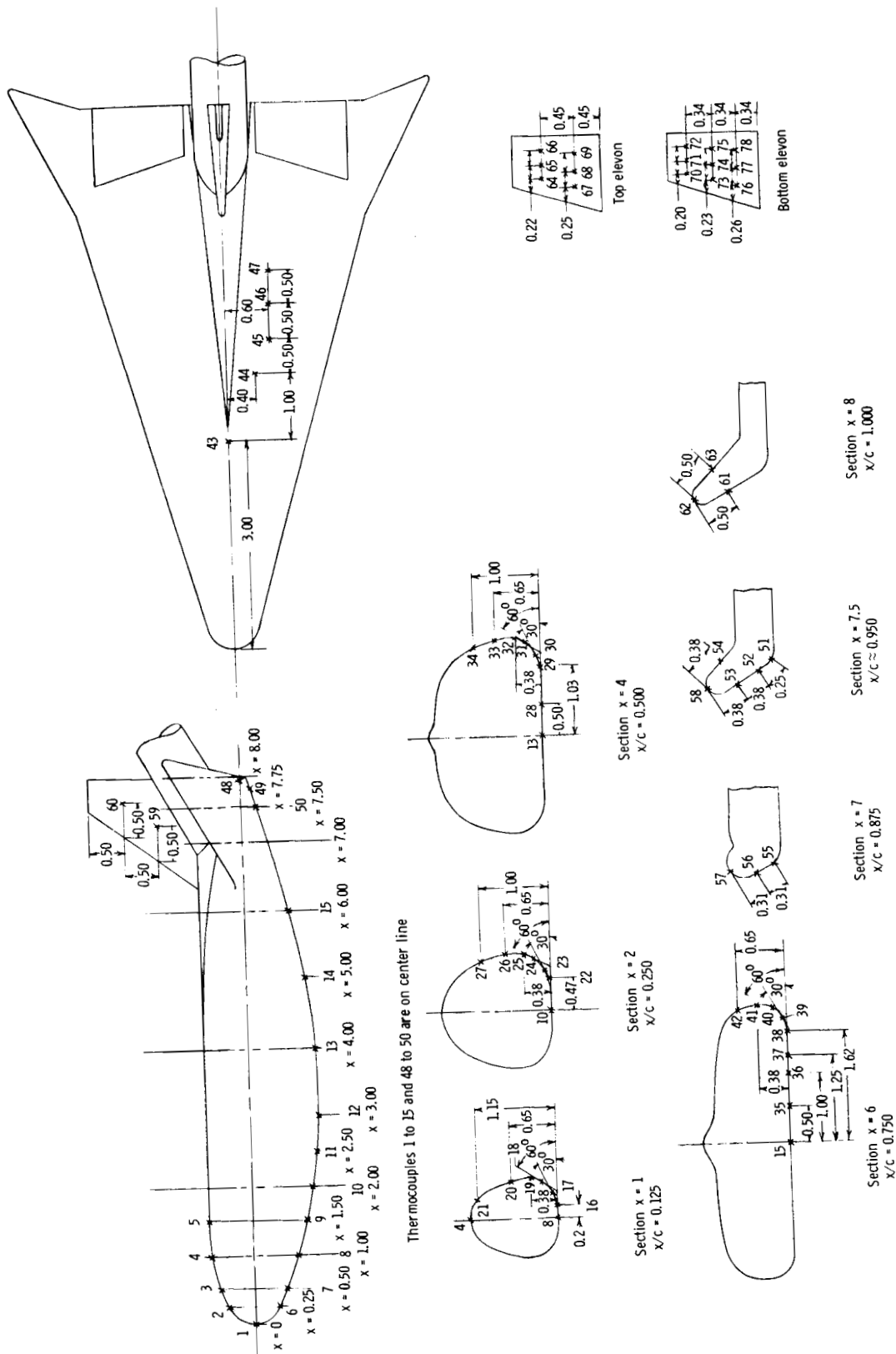
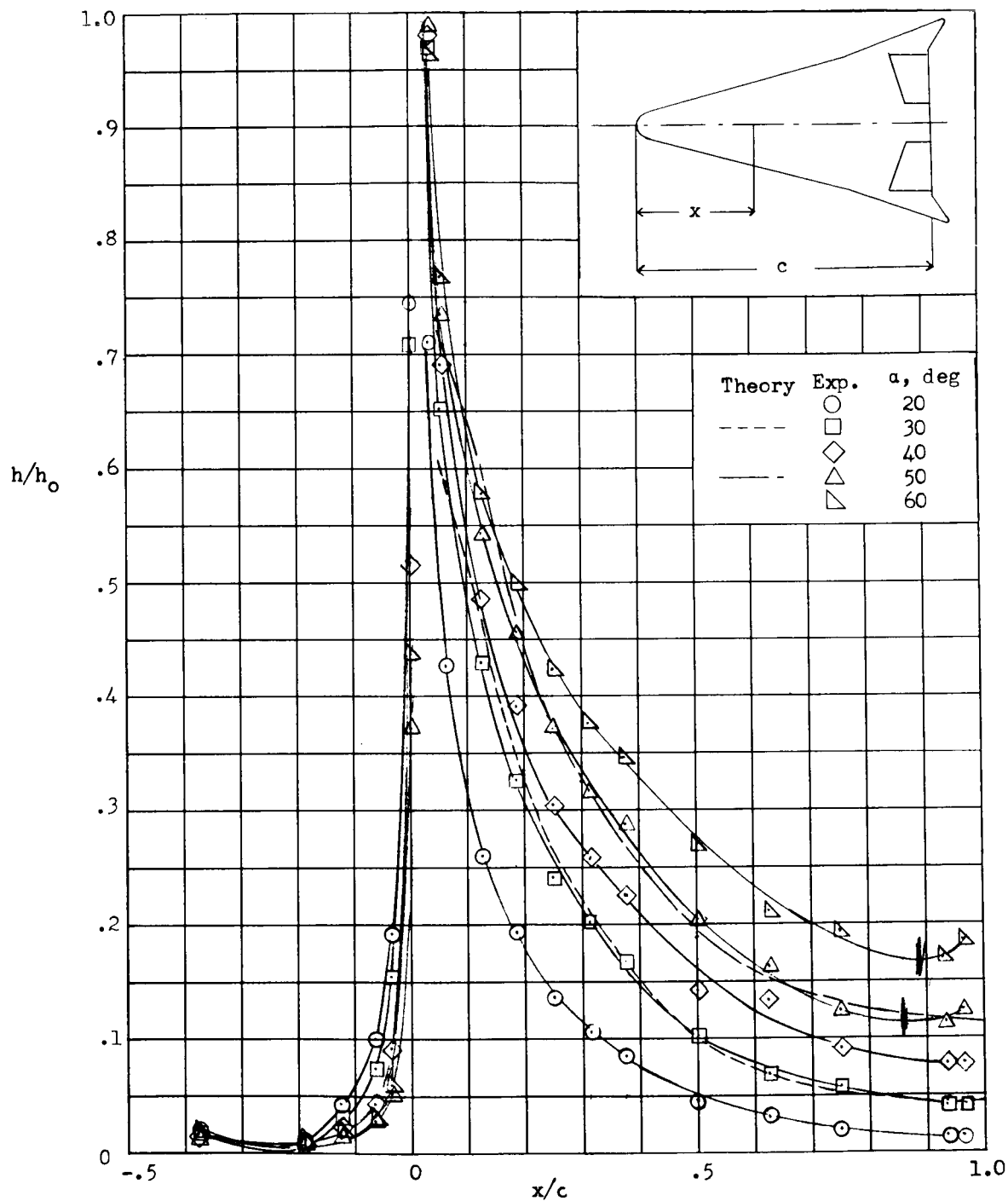


Figure 3.- HL-10 heat-transfer model thermocouple locations. All dimensions are in inches.

UNCLASSIFIED

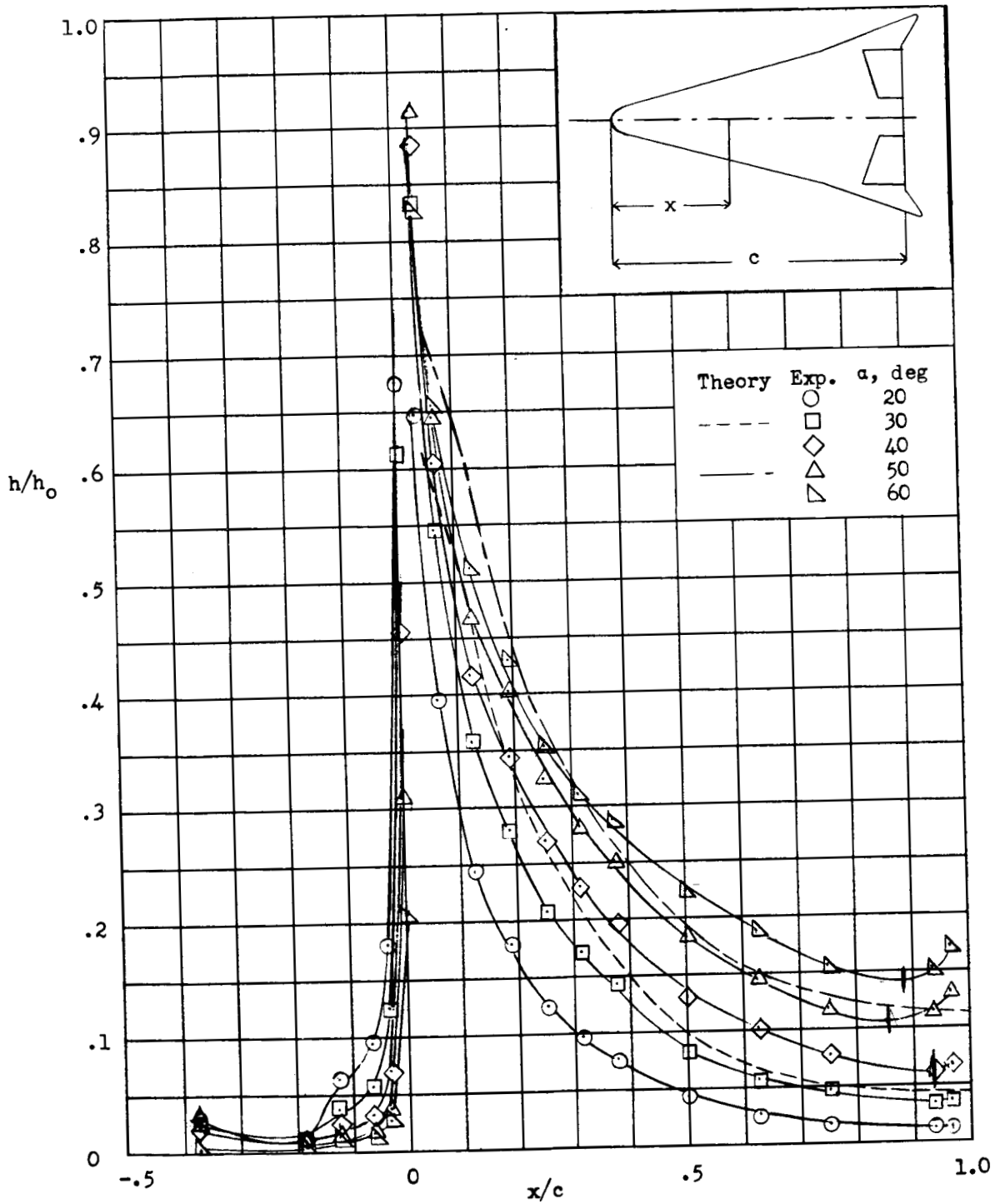


(a)  $R_c = 0.24 \times 10^6$ .

Figure 4.- Variation of heat transfer along center line for angles of attack from 20° to 60°.  $\delta_e = 0^\circ$ .

UNCLASSIFIED

~~CONFIDENTIAL~~

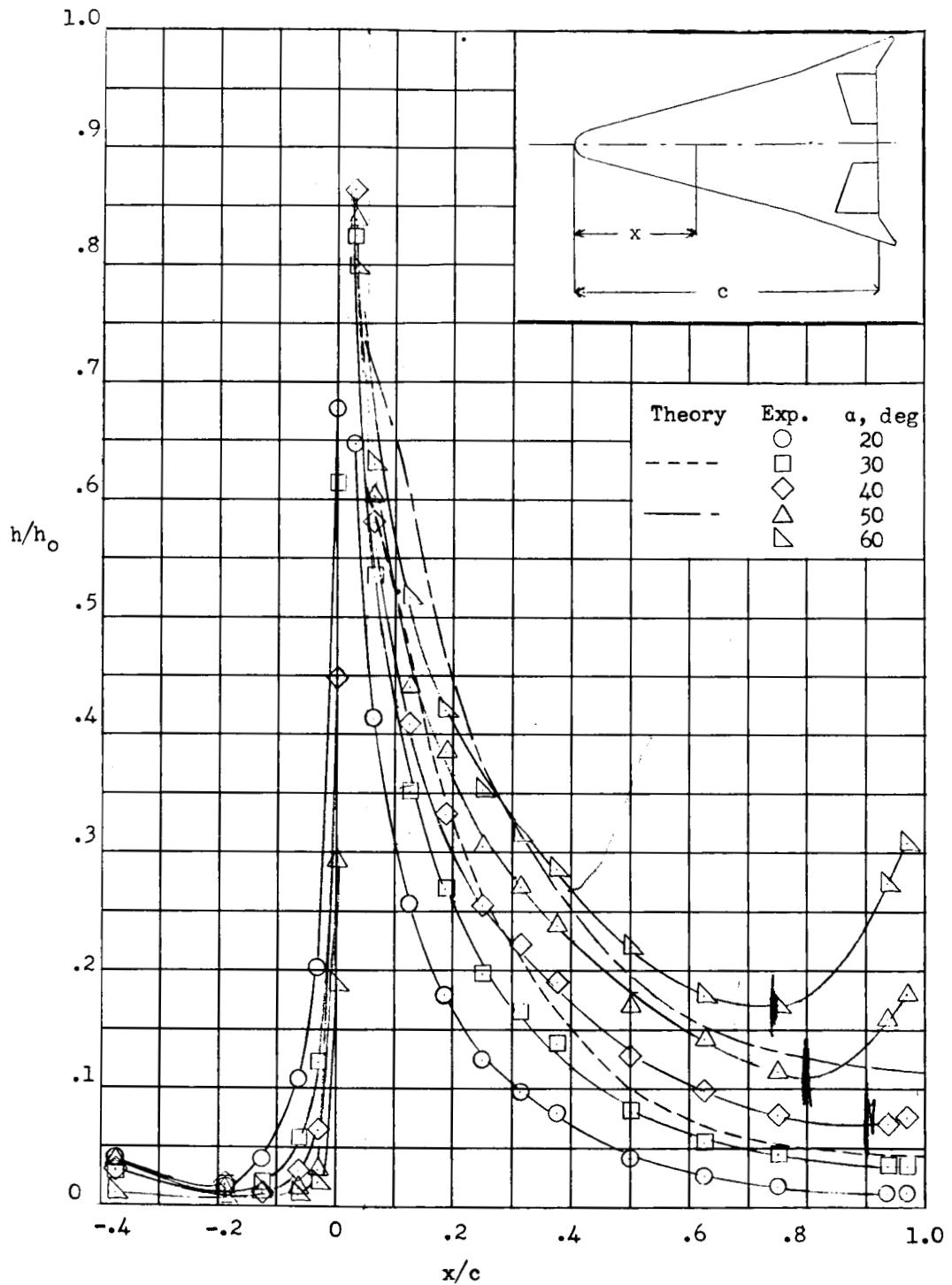


(b)  $R_c = 0.77 \times 10^6$ .

Figure 4.- Continued.

~~CONFIDENTIAL~~

UNCLASSIFIED

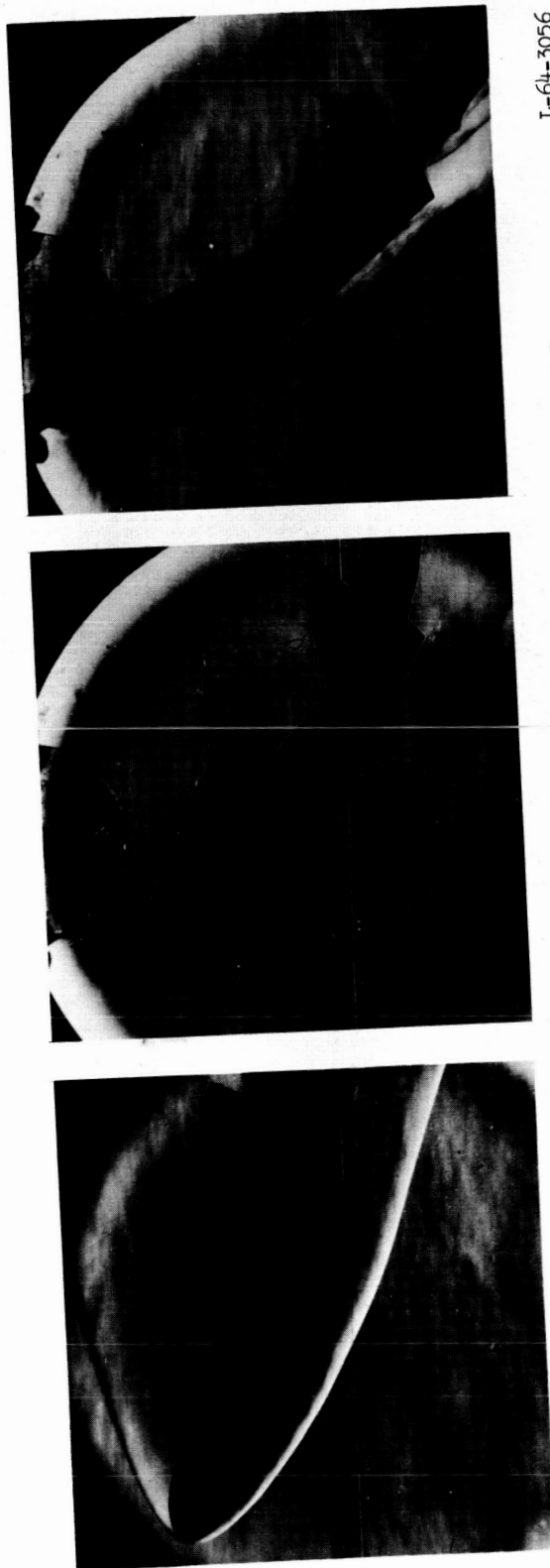


(c)  $Re = 2.70 \times 10^6$ .

Figure 4.- Concluded.

UNCLASSIFIED

~~CONFIDENTIAL~~



L-64-3056

(c)  $\alpha = 60^\circ$ .

(b)  $\alpha = 40^\circ$ .

(a)  $\alpha = 20^\circ$ .

Figure 5.- Side-view schlieren photographs of model at various angles of attack.  $\delta_e = 0^\circ$ ;  $M_\infty = 8$ .

~~CONFIDENTIAL~~

UNCLASSIFIED

~~CONFIDENTIAL~~

I-64-3057

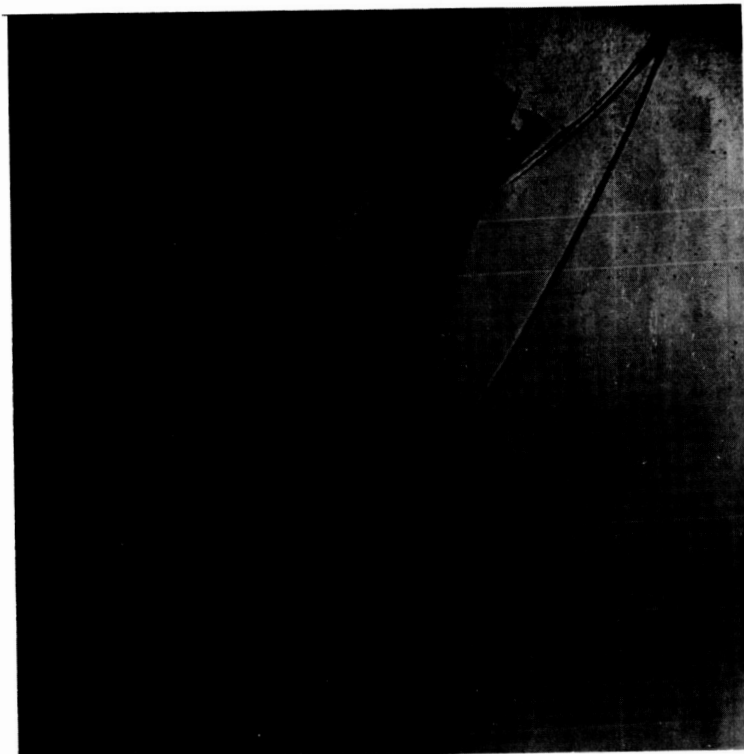
(b)  $\alpha = 50^\circ$ ;  $\delta_e = -60^\circ$ .(a)  $\alpha = 30^\circ$ ;  $\delta_e = 30^\circ$ .

Figure 6.- Side-view schlieren photographs of model with elevons deflected.  $M_\infty = 8$ ;  $R_c = 2.70 \times 10^6$ .

~~CONFIDENTIAL~~

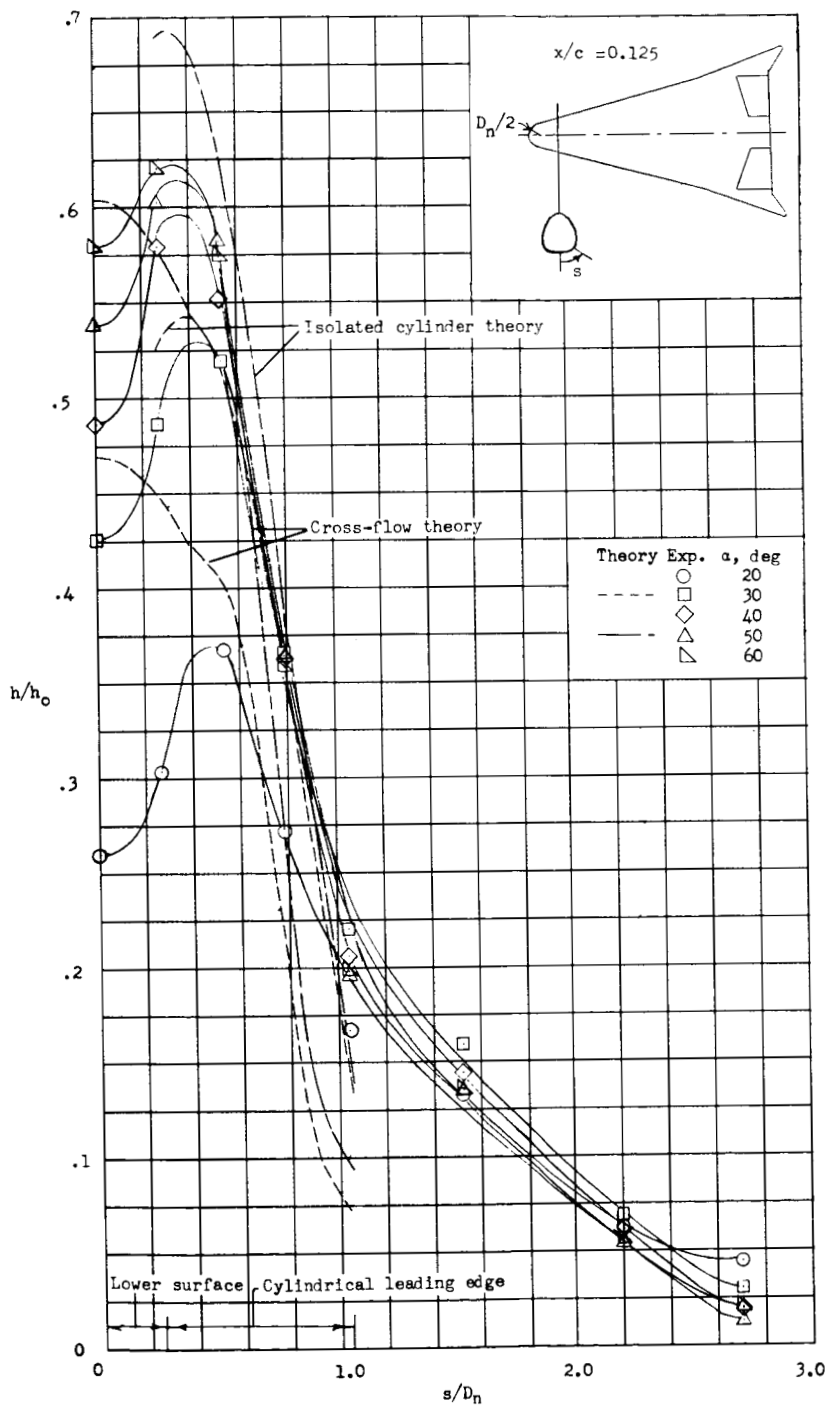
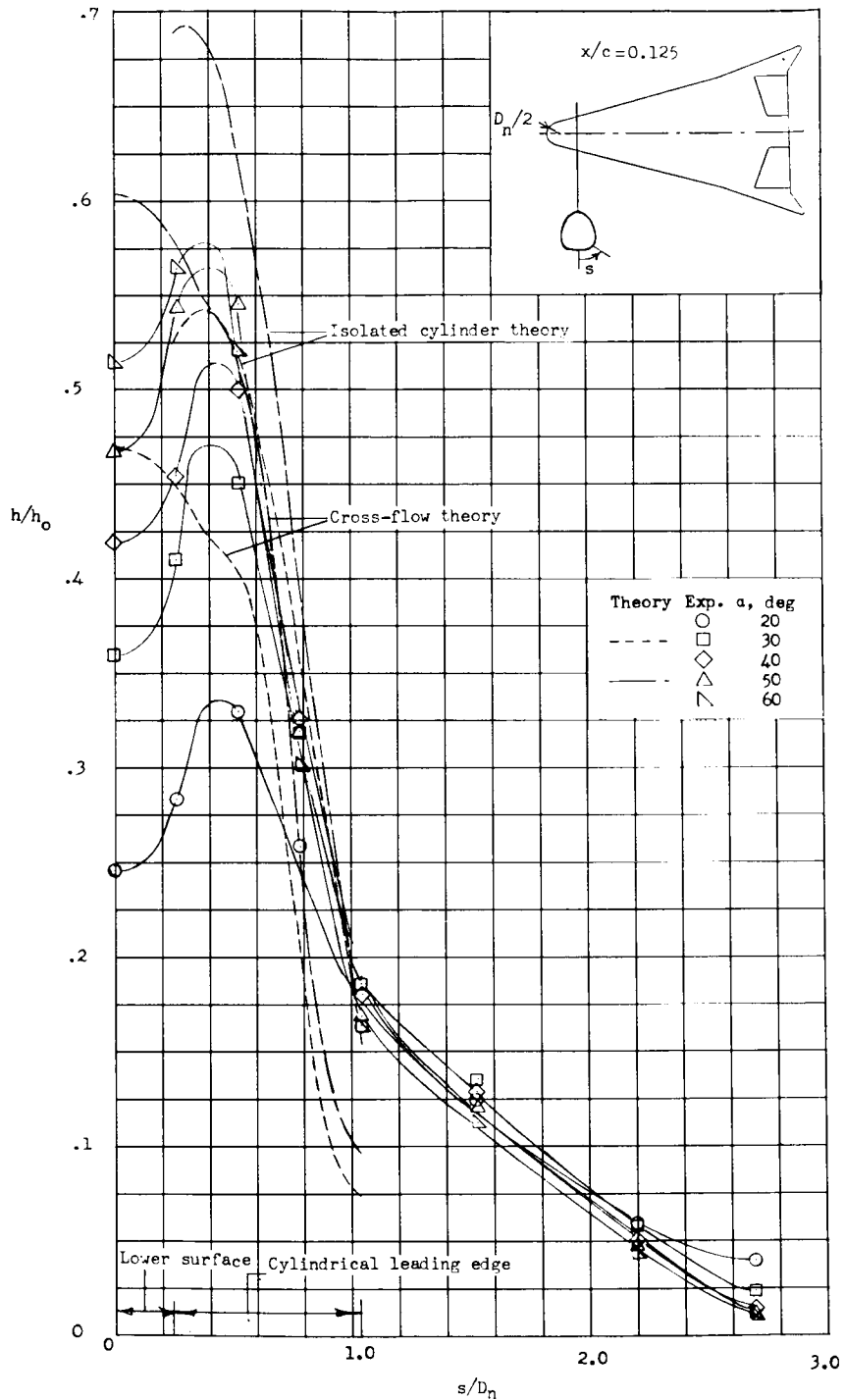
~~CONFIDENTIAL~~(a)  $Re = 0.24 \times 10^6$ .

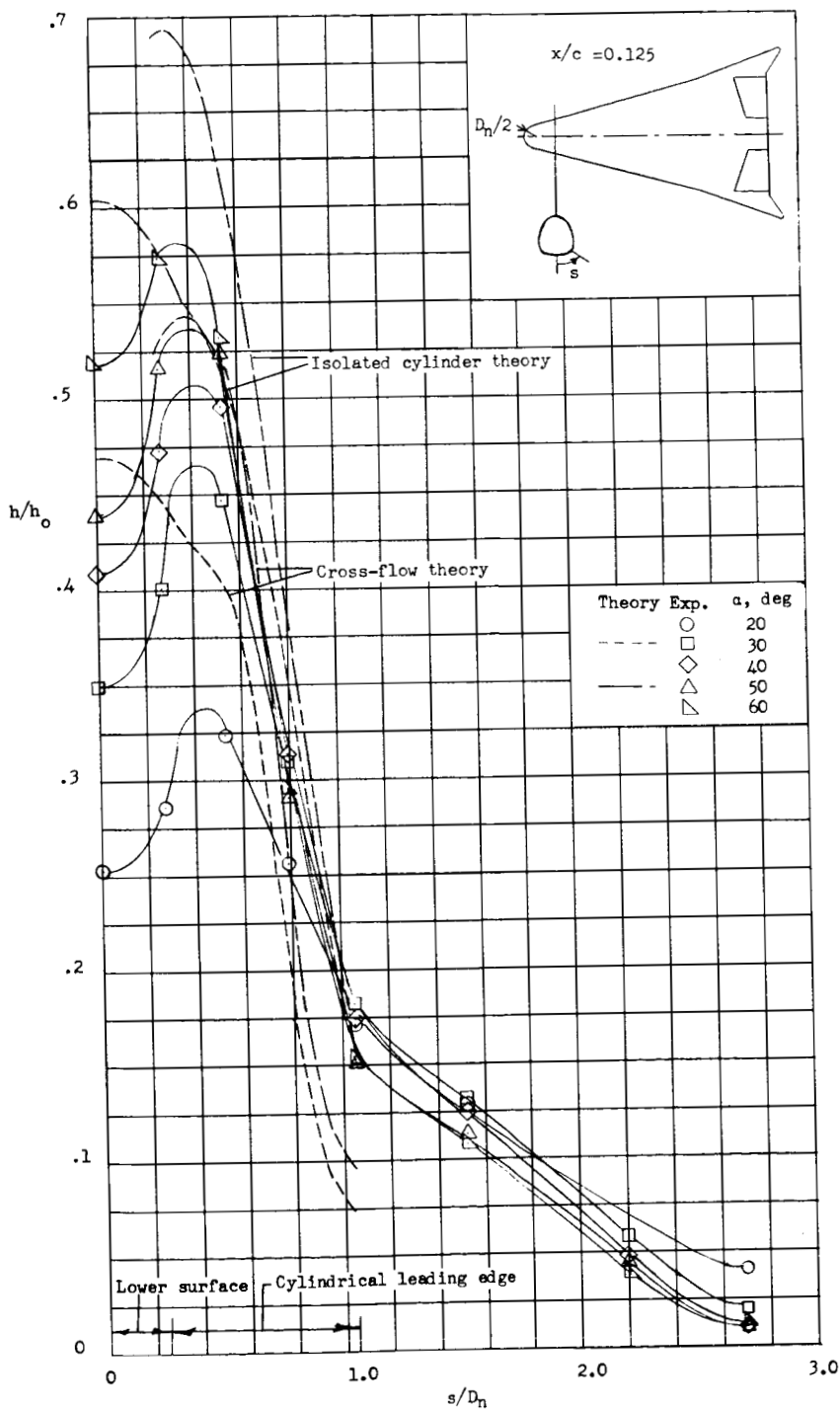
Figure 7.- Spanwise distribution of heat transfer at station  $x/c = 0.125$  at angles of attack from  $20^\circ$  to  $60^\circ$ .  $\delta_e = 0^\circ$ .

~~CONFIDENTIAL~~



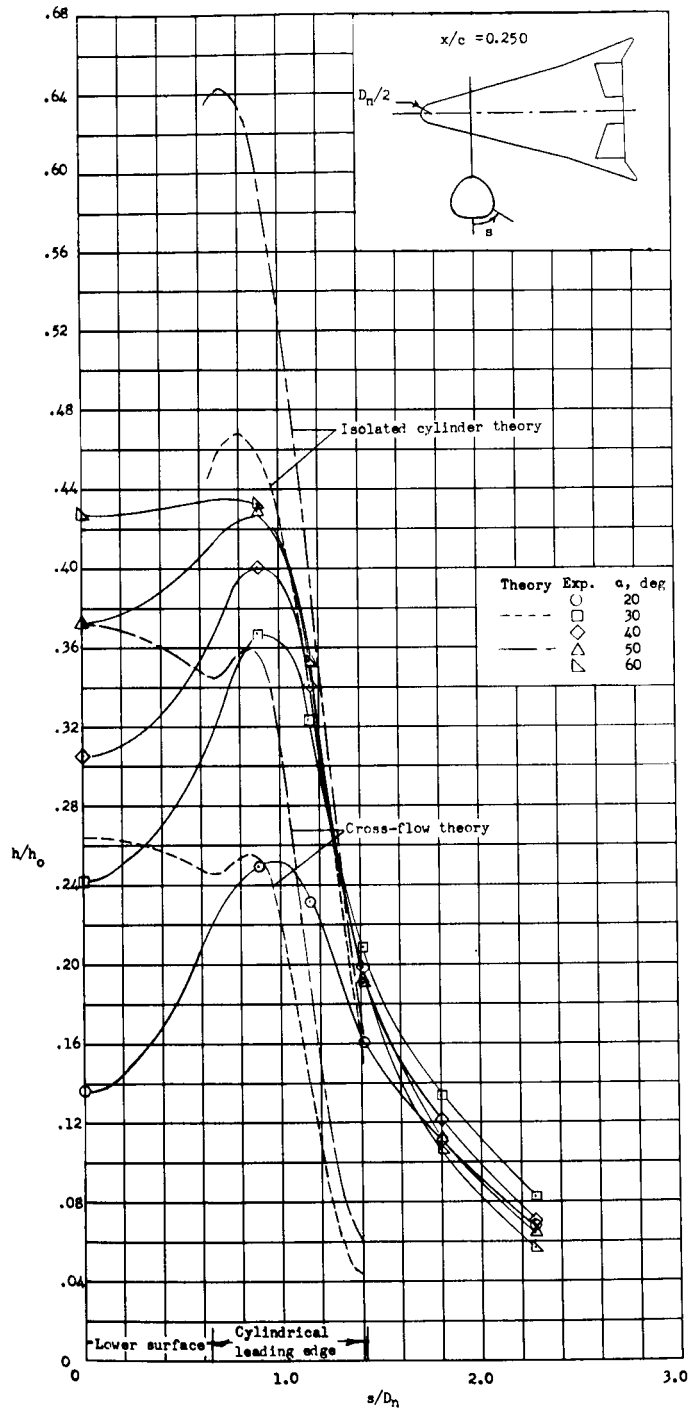
(b)  $R_c = 0.77 \times 10^6$ .

Figure 7.- Continued.



(c)  $R_c = 2.70 \times 10^6$ .

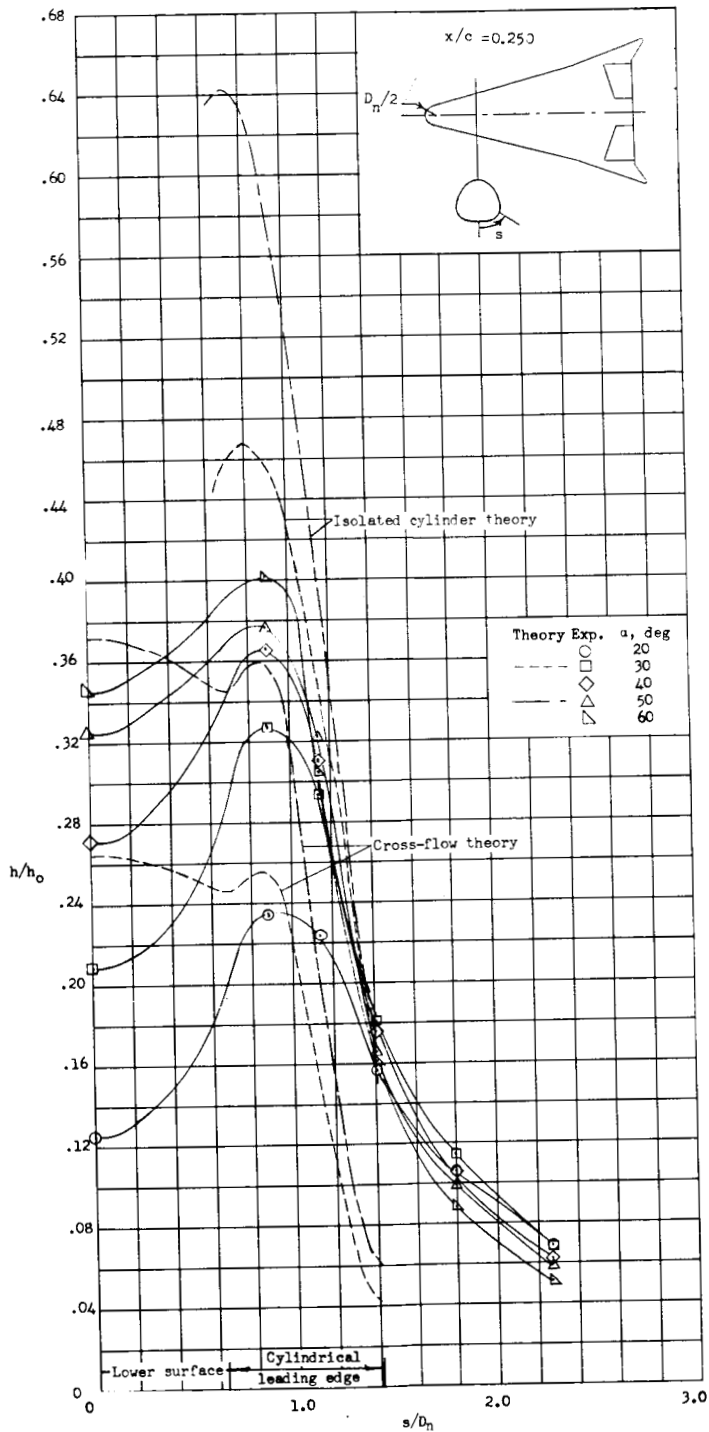
Figure 7.- Concluded.



(a)  $R_c = 0.24 \times 10^6$ .

Figure 8.- Spanwise distribution of heat transfer at station  $x/c = 0.250$  at angles of attack from  $20^\circ$  to  $60^\circ$ .  $\delta_e = 0^\circ$ .

UNCLASSIFIED

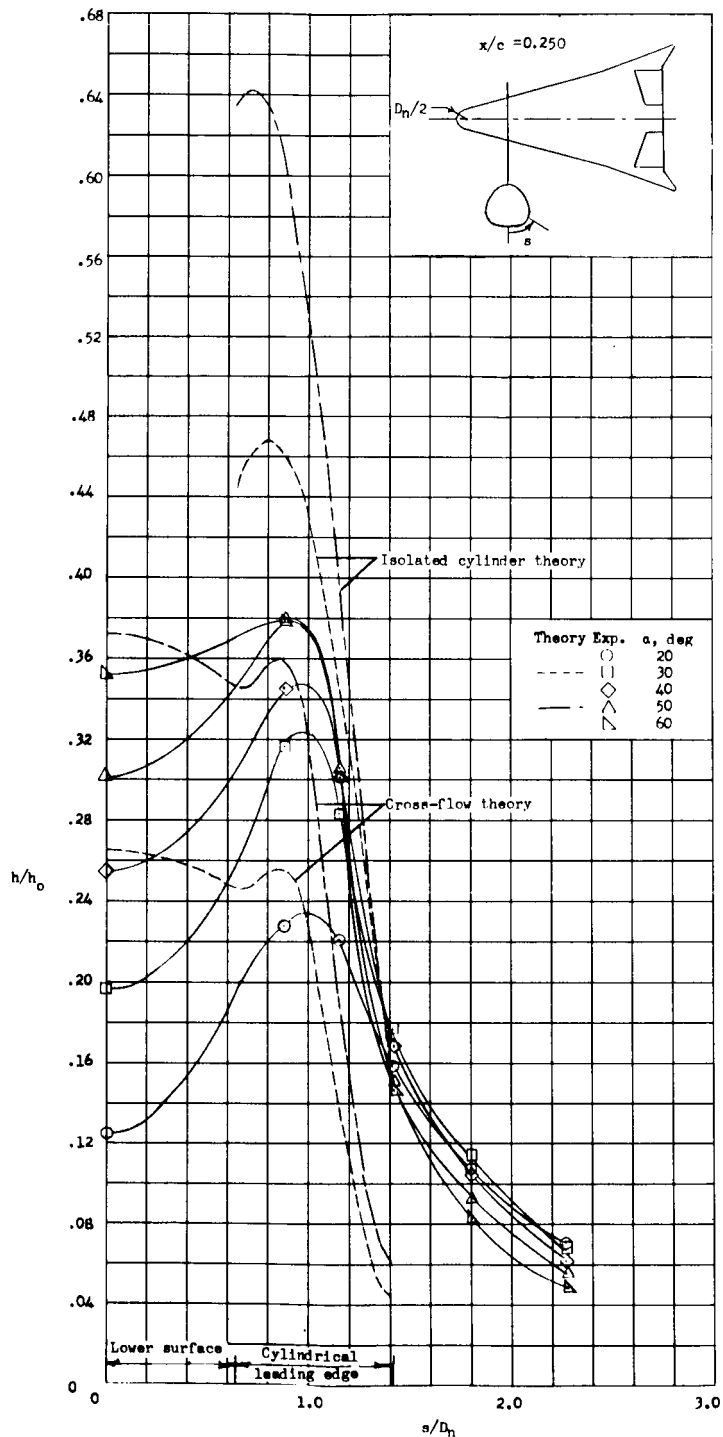


(b)  $R_c = 0.77 \times 10^6$ .

Figure 8.- Continued.

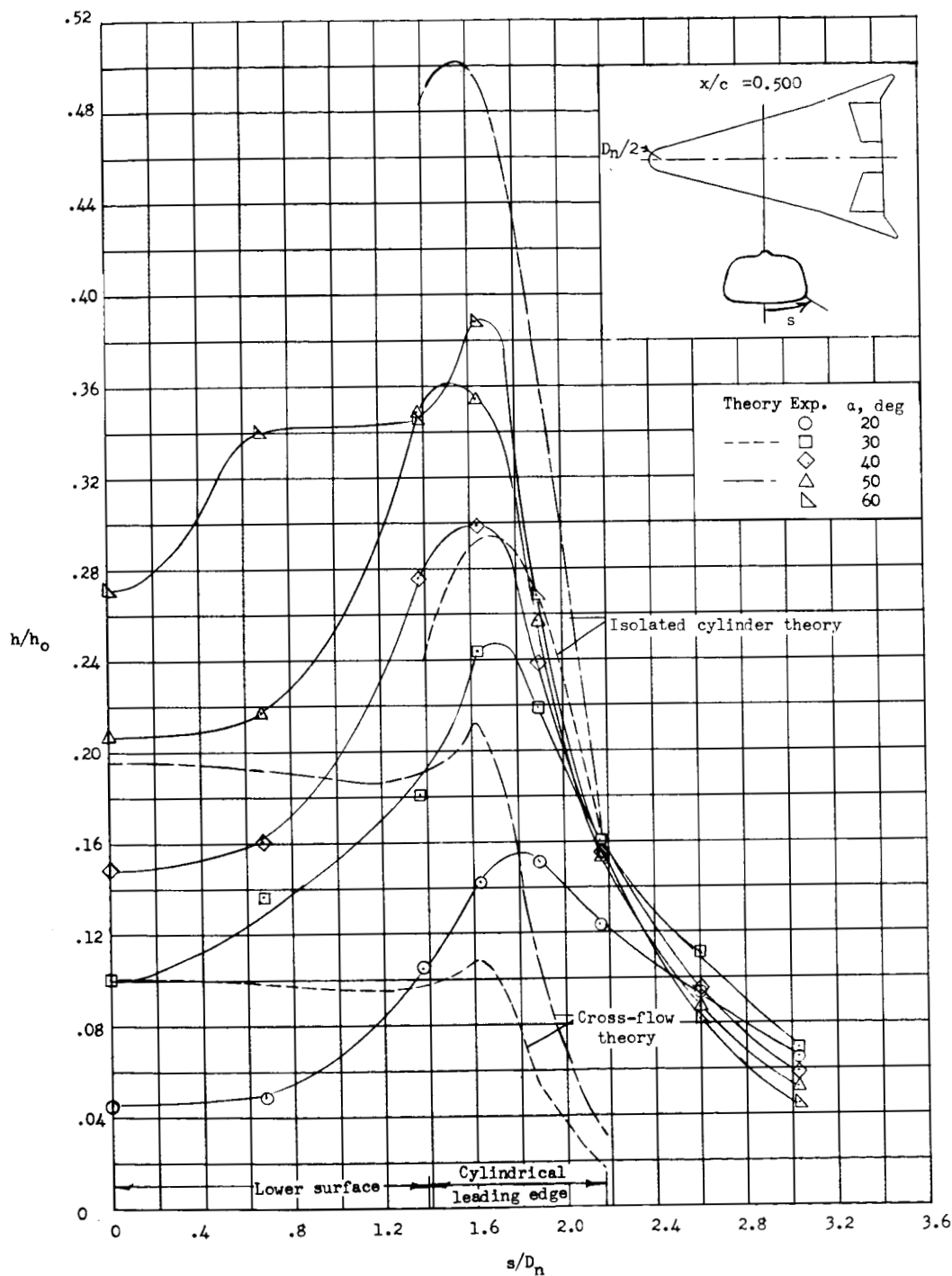
CONFIDENTIAL

UNCLASSIFIED



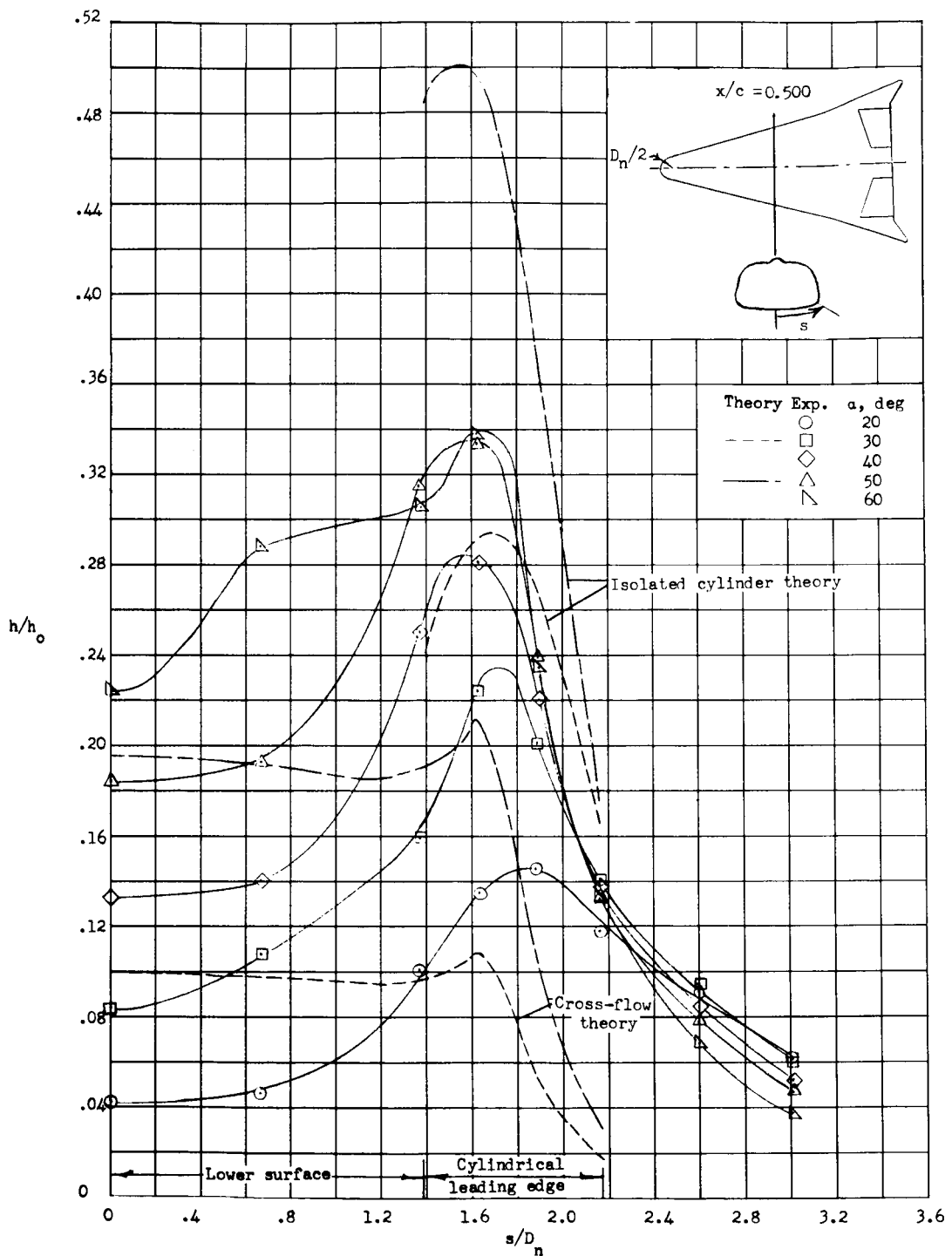
(c)  $R_c = 2.70 \times 10^6$ .

Figure 8.- Concluded.



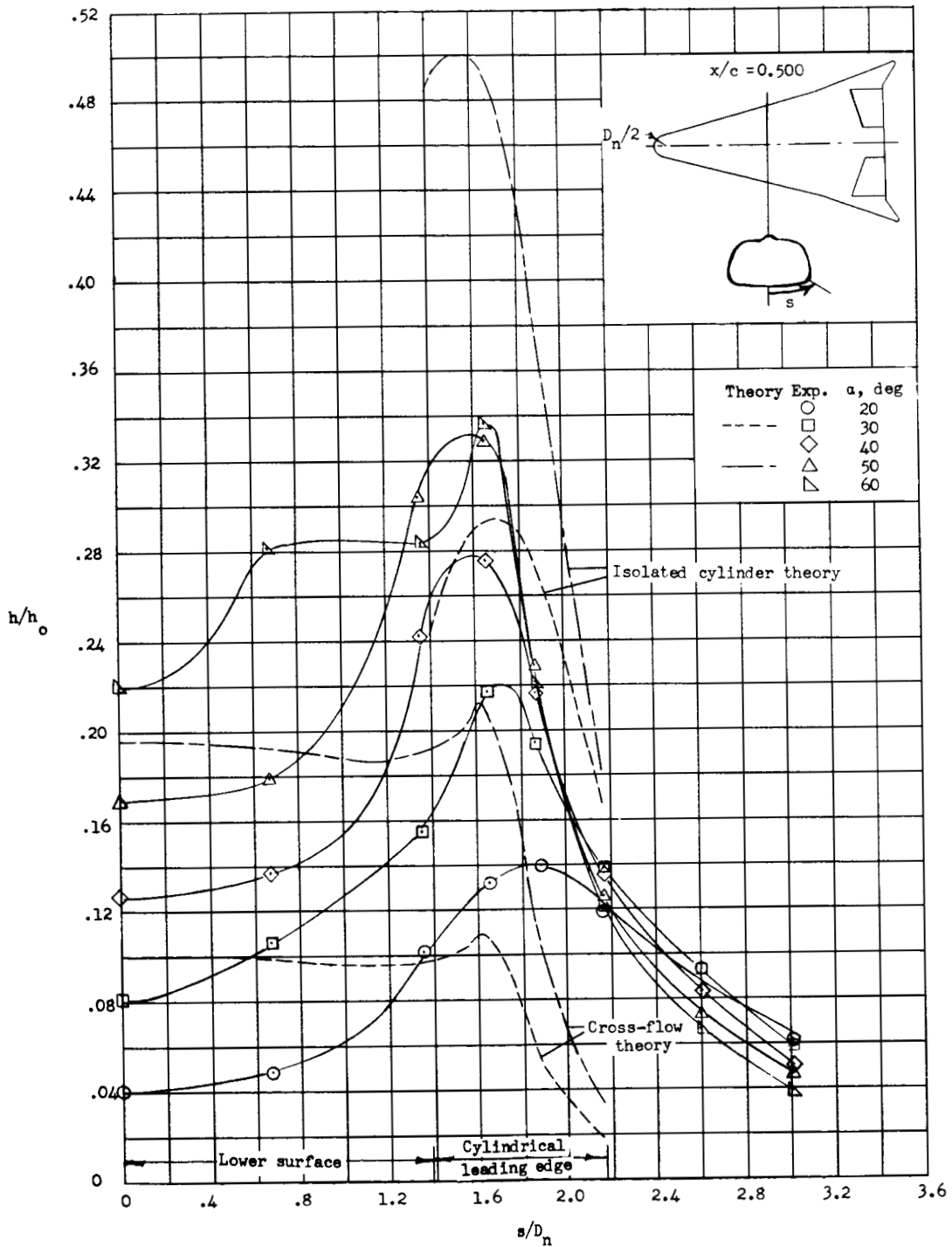
(a)  $Re = 0.24 \times 10^6$ .

Figure 9.- Spanwise distribution of heat transfer at station  $x/c = 0.500$  at angles of attack from  $20^\circ$  to  $60^\circ$ .  $\delta_e = 0^\circ$ .



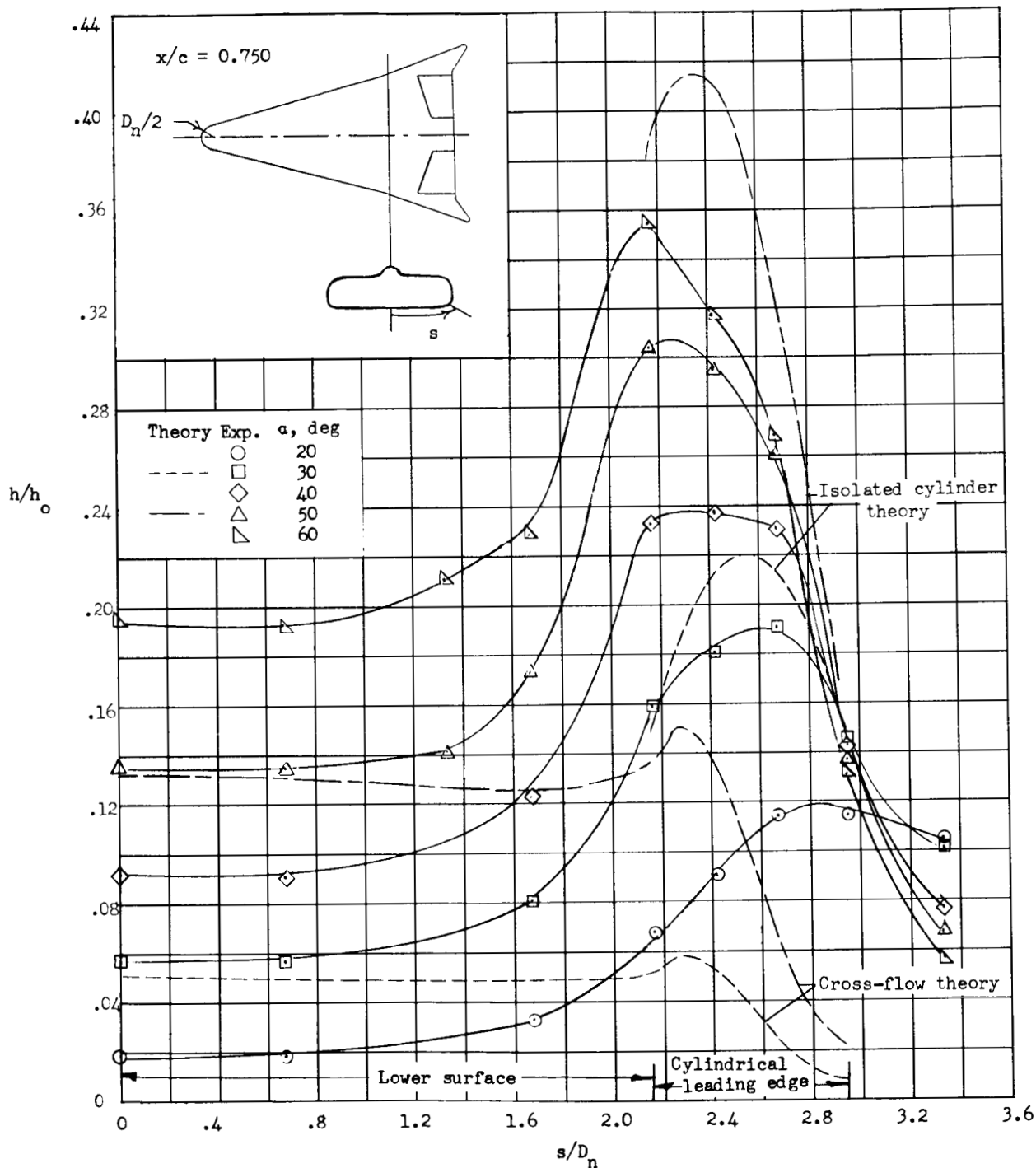
(b)  $R_c = 0.77 \times 10^6$ .

Figure 9.- Continued.



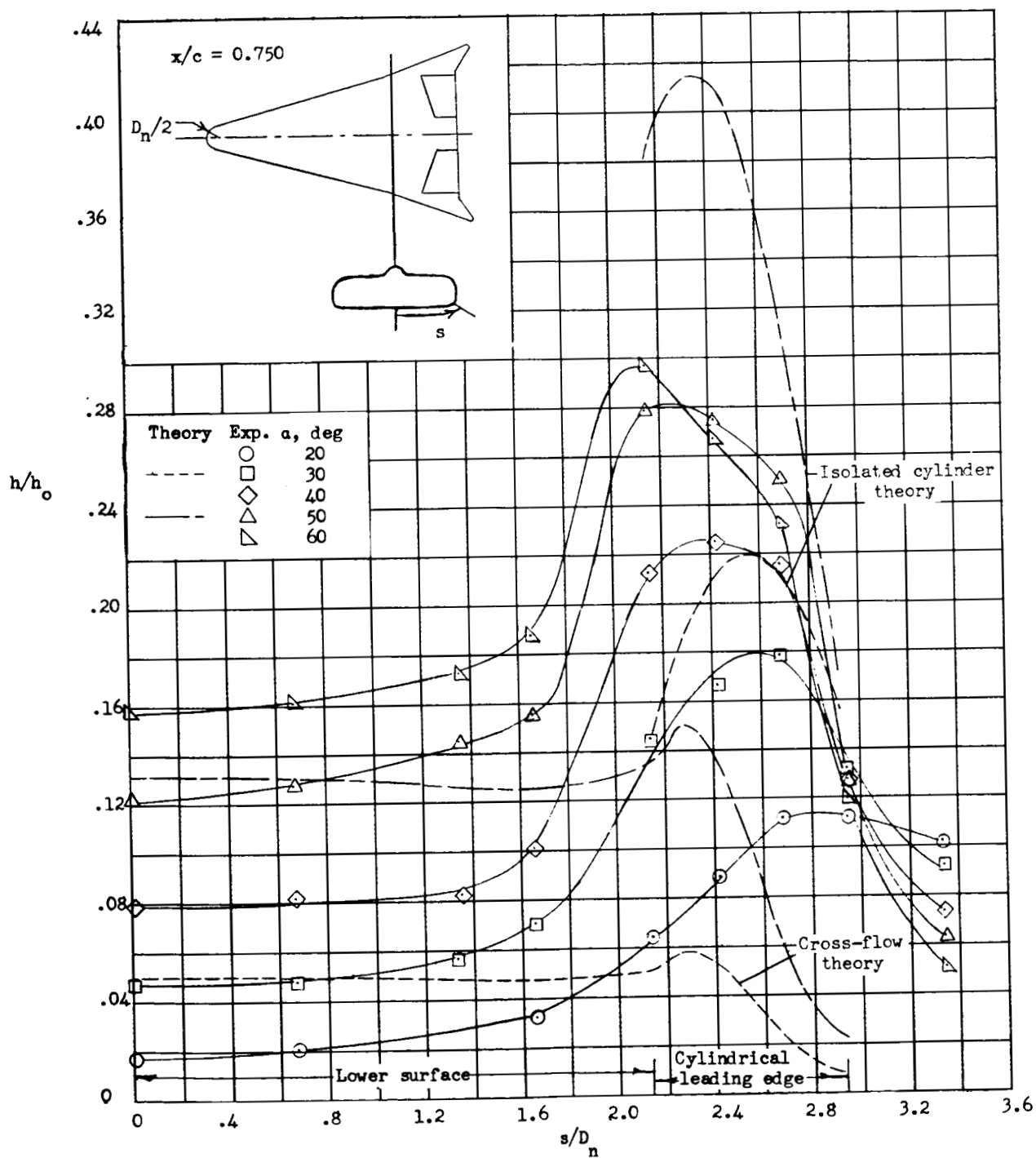
(c)  $R_c = 2.70 \times 10^6$ .

Figure 9.- Concluded.



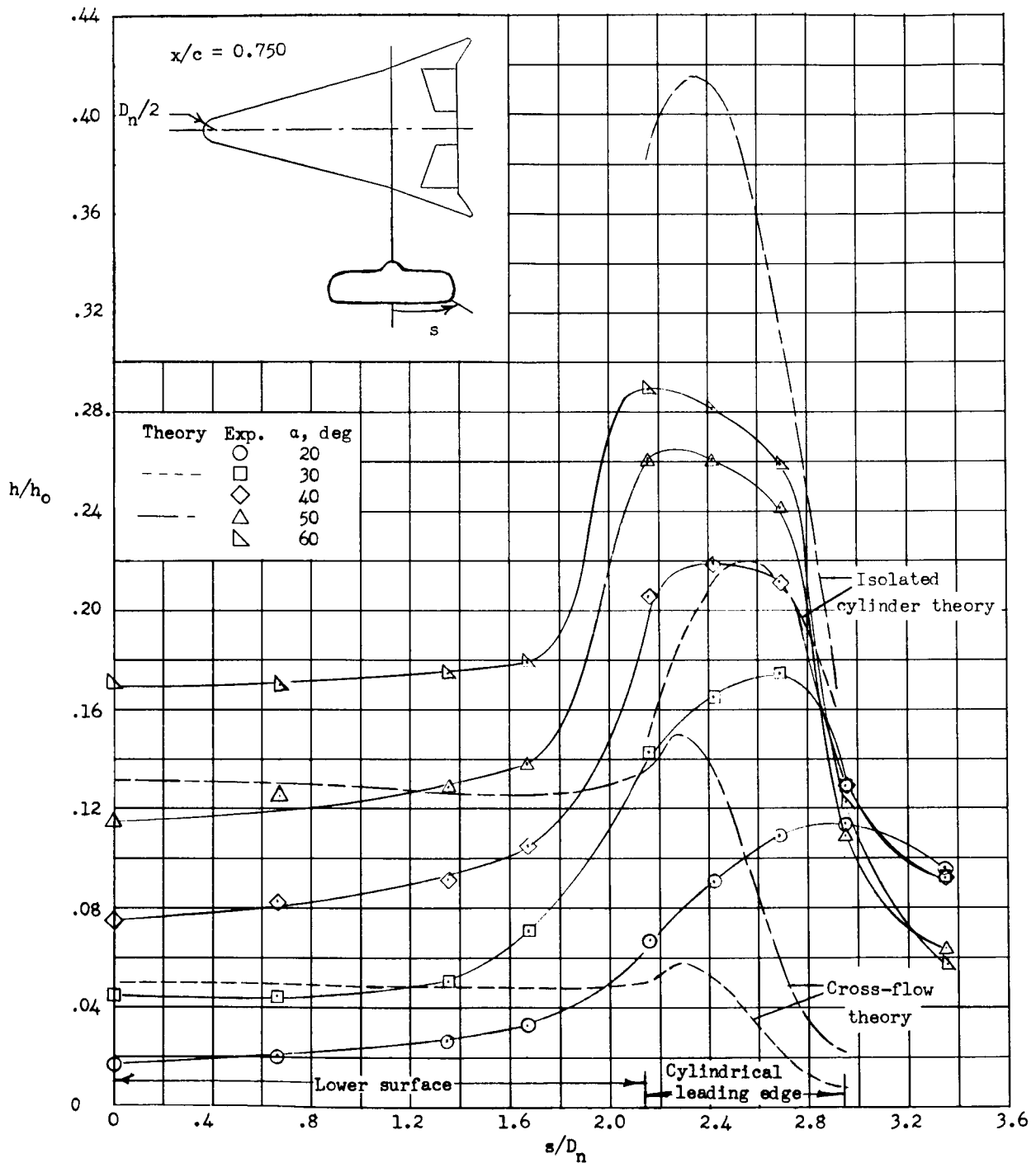
(a)  $R_c = 0.24 \times 10^6$ .

Figure 10.- Spanwise distribution of heat transfer at station  $x/c = 0.750$  at angles of attack from  $20^\circ$  to  $60^\circ$ .  $\delta_e = 0^\circ$ .



(b)  $R_c = 0.77 \times 10^6$ .

Figure 10.- Continued.

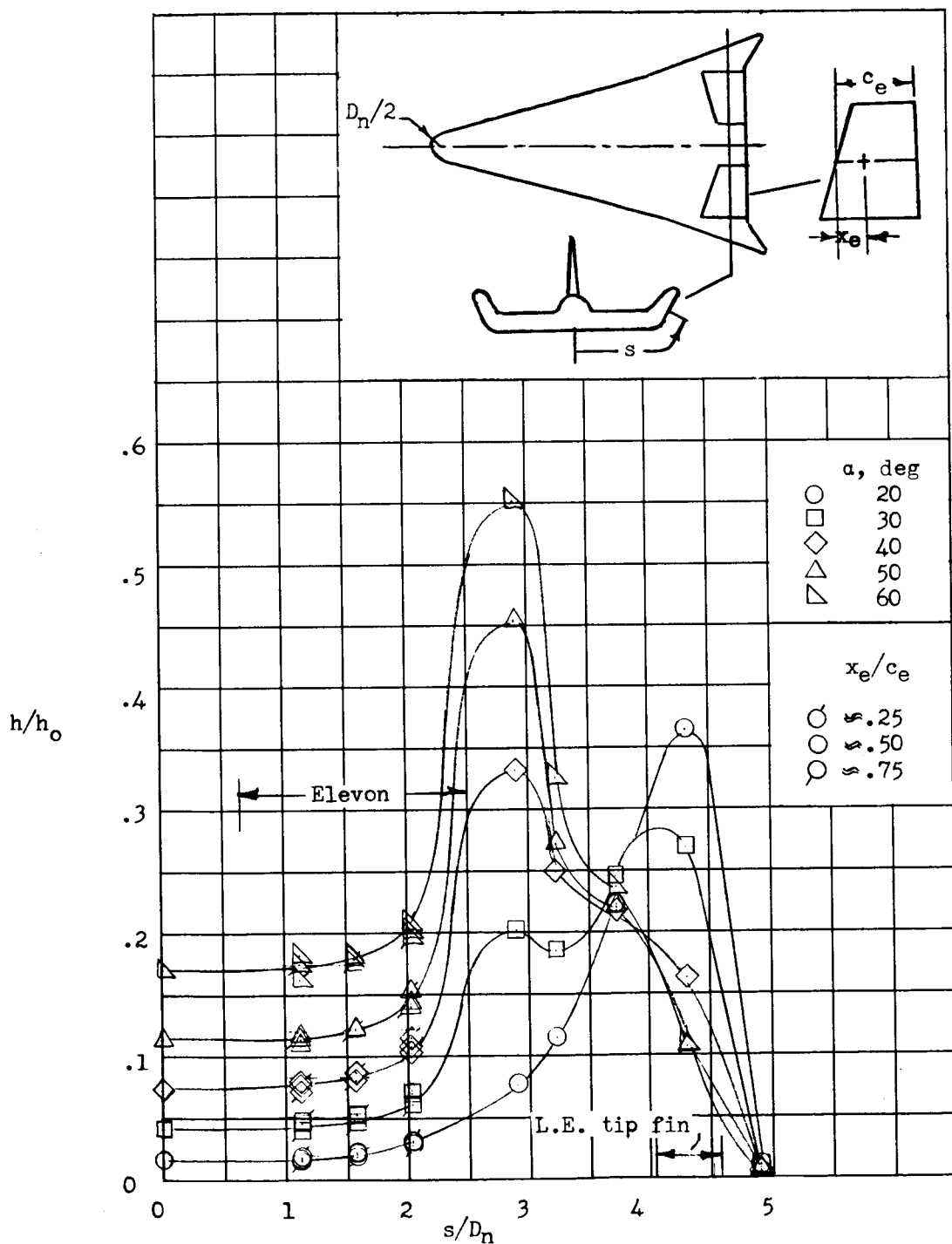


(c)  $R_c = 2.70 \times 10^6$ .

Figure 10.- Concluded.

UNCLASSIFIED

CONFIDENTIAL

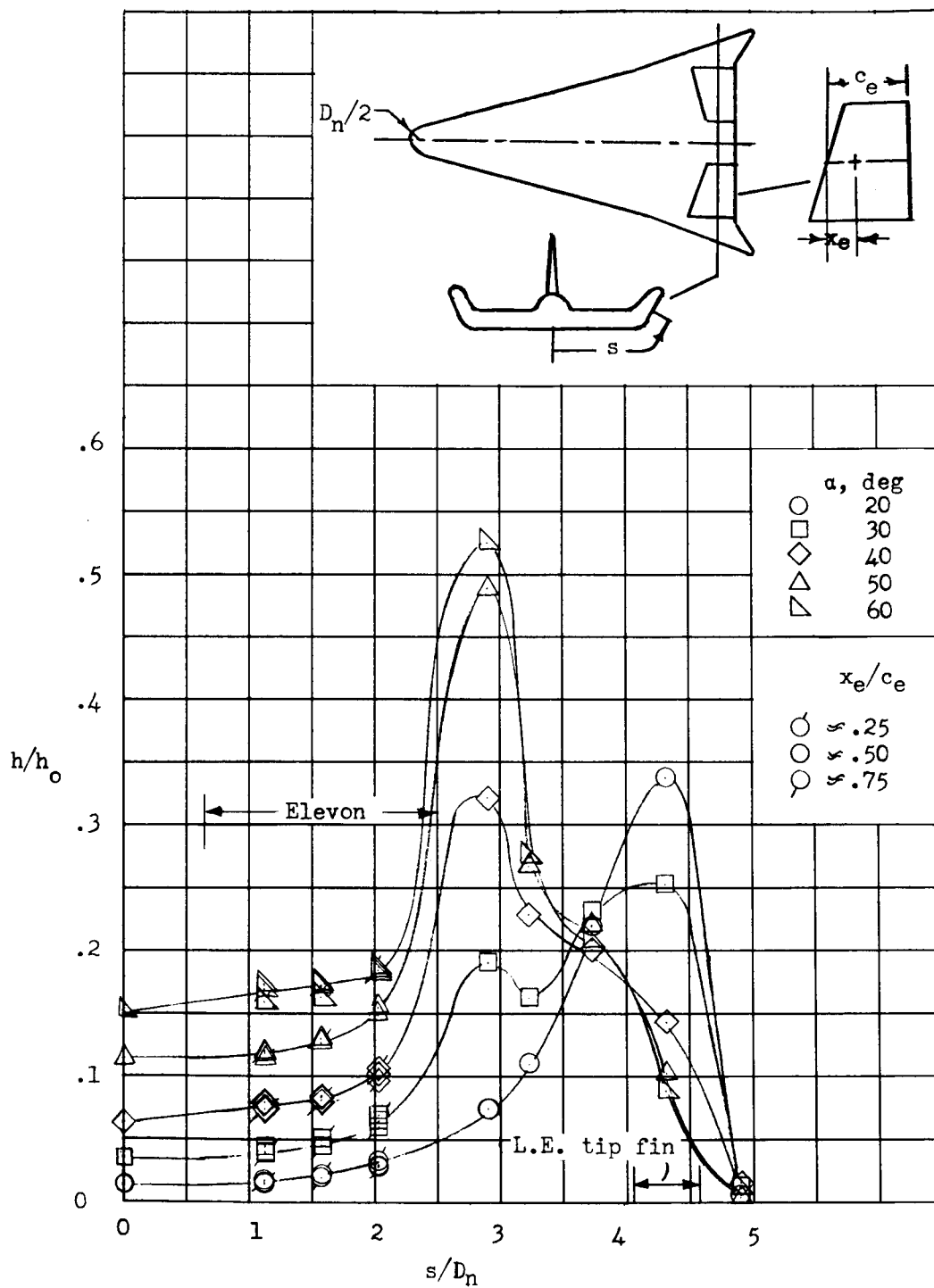


(a)  $Re = 0.24 \times 10^6$ .

Figure 11.- Spanwise distribution of heat transfer at station  $x/c \approx 0.950$  at angles of attack from  $20^\circ$  to  $60^\circ$ .  $\delta_e = 0^\circ$ .

CONFIDENTIAL

UNCLASSIFIED

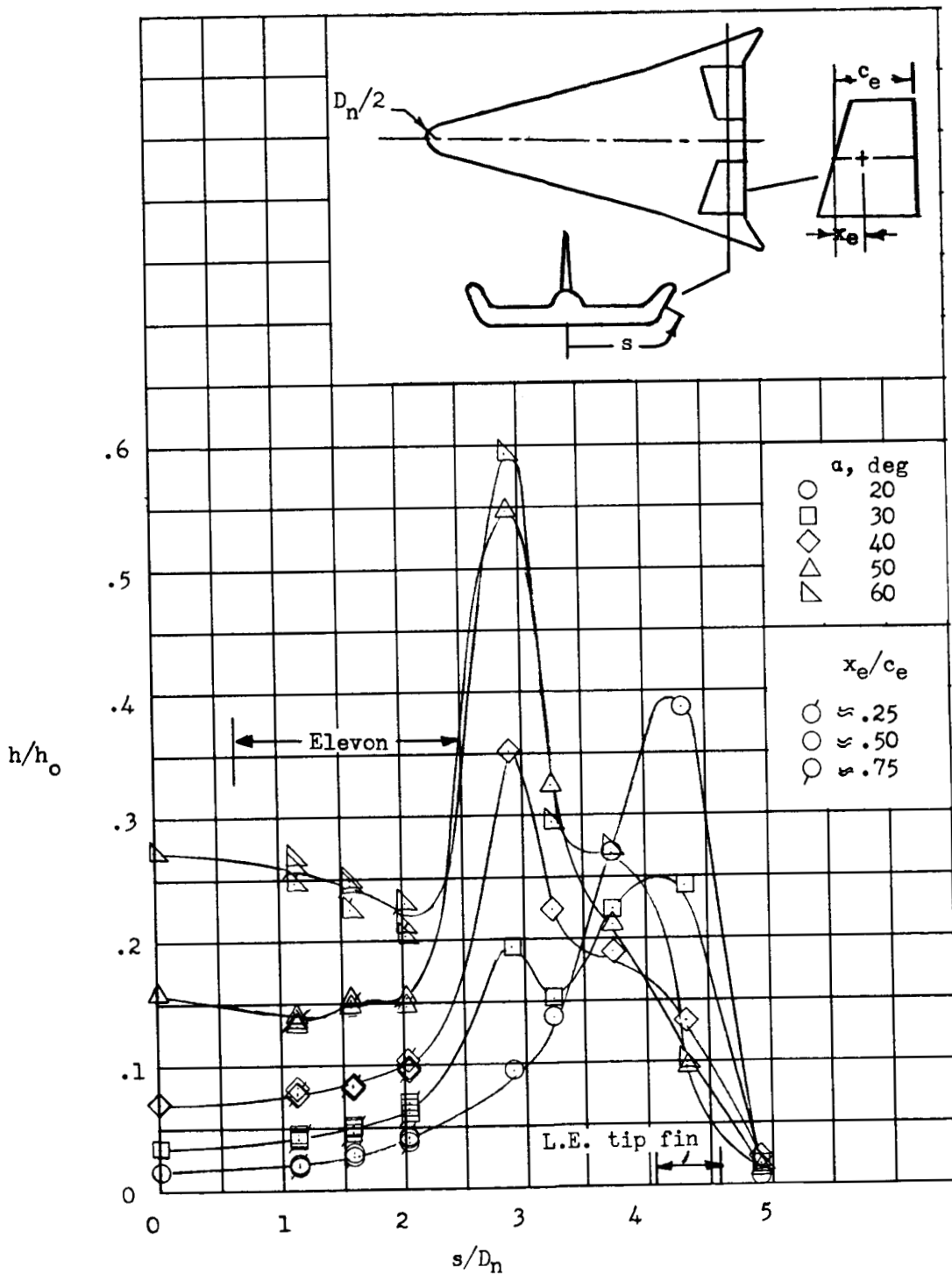


(b)  $R_c = 0.77 \times 10^6$ .

Figure 11.- Continued.

# UNCLASSIFIED

~~CONFIDENTIAL~~



(c)  $R_c = 2.70 \times 10^6$ .

Figure 11.- Concluded:

~~CONFIDENTIAL~~  
UNCLASSIFIED

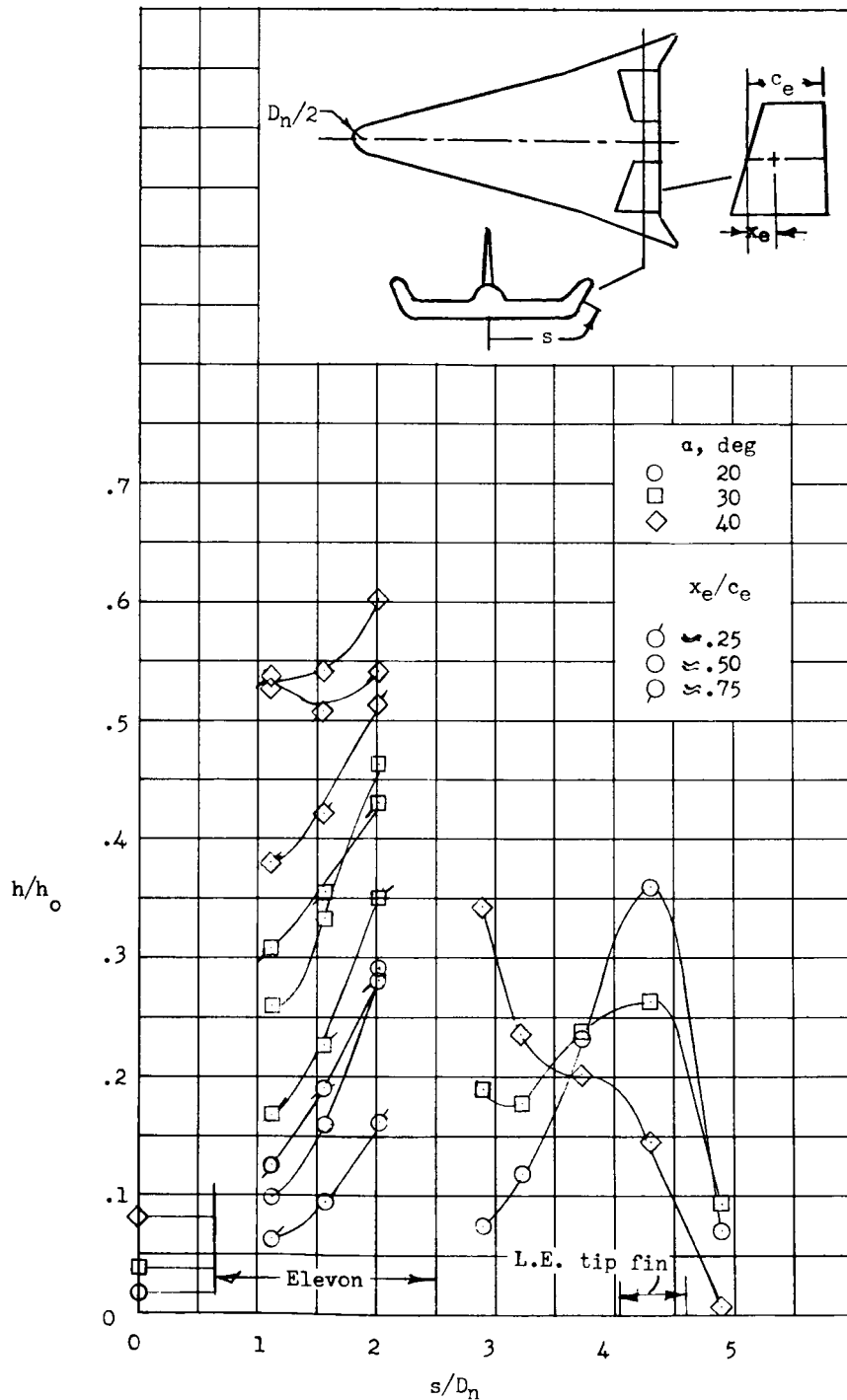
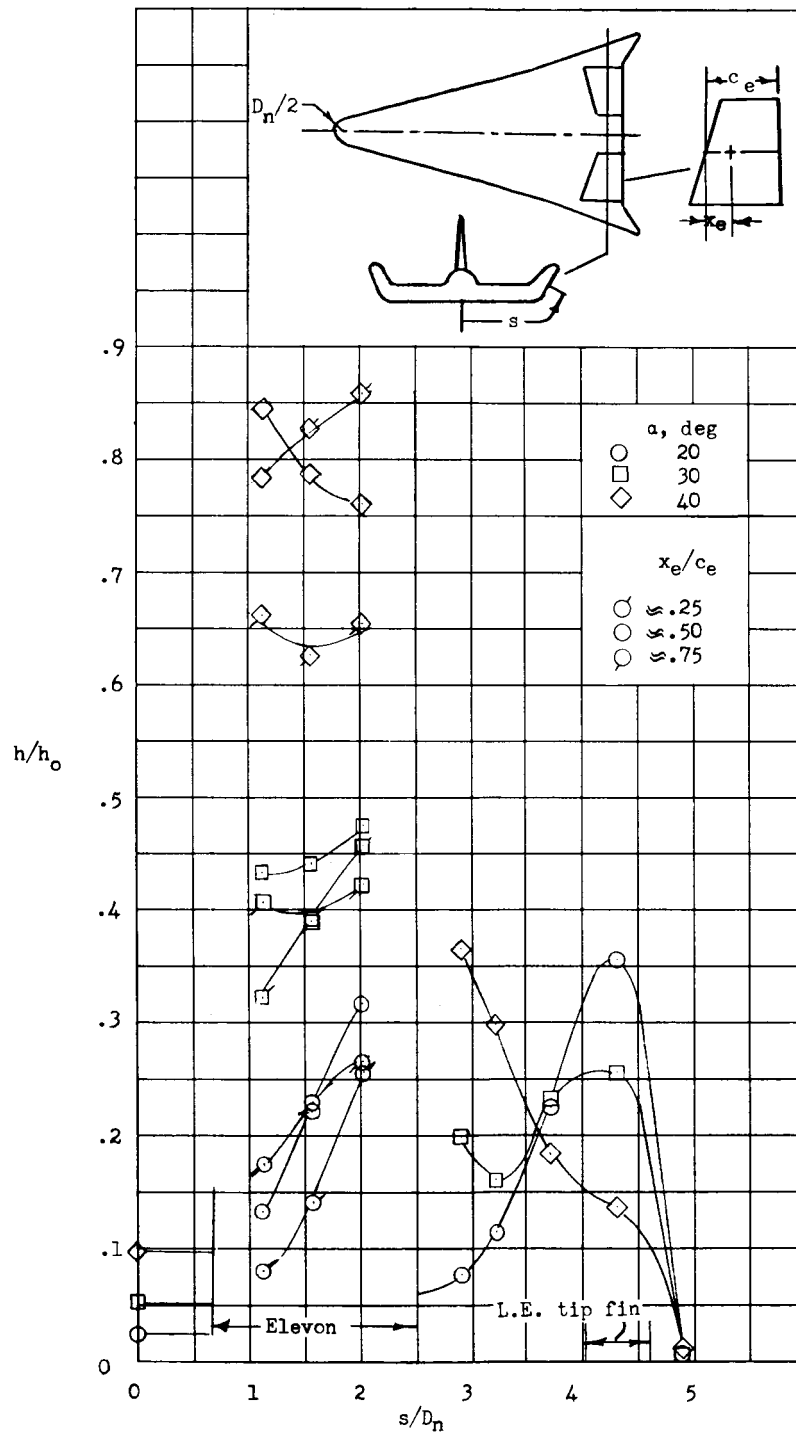
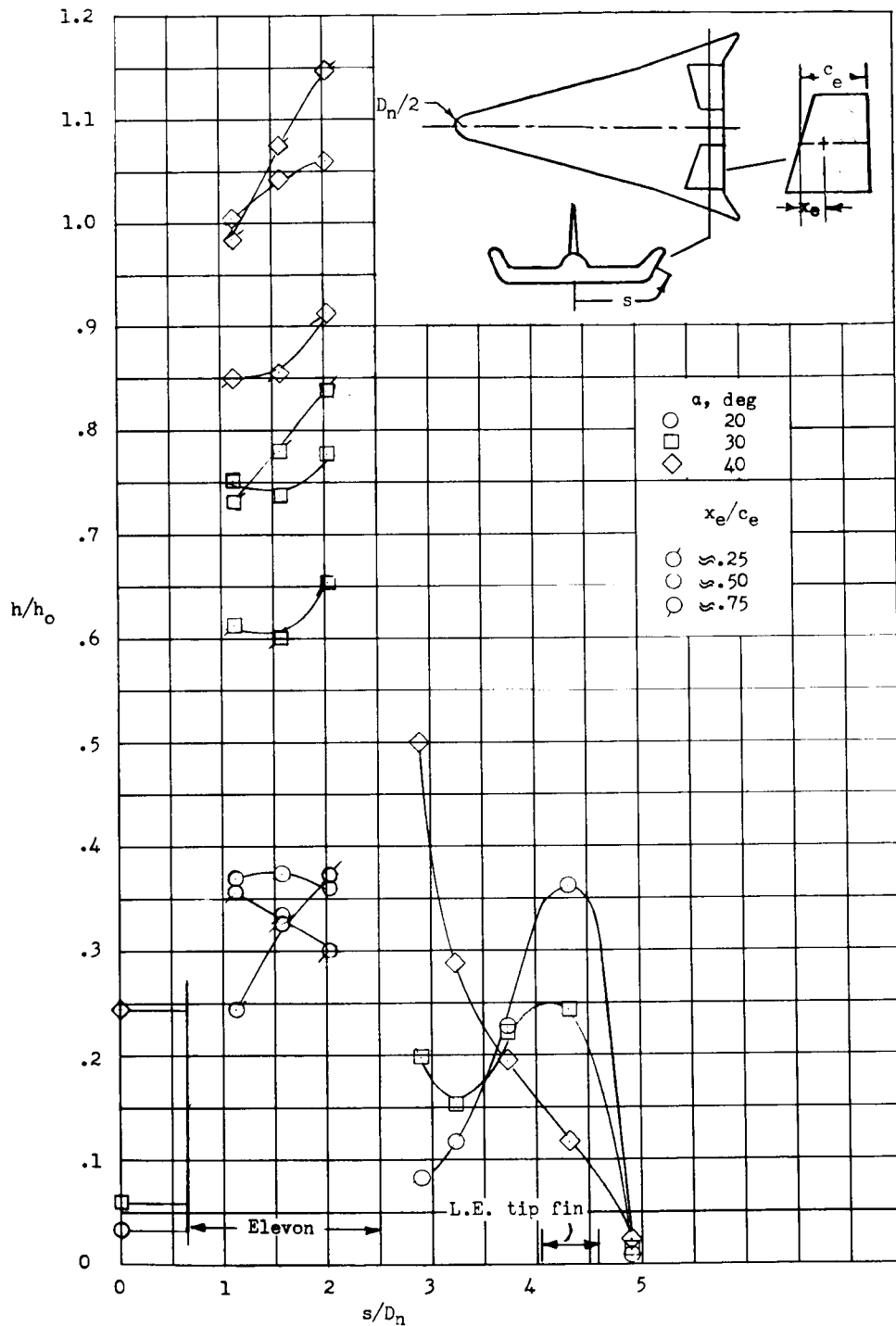


Figure 12.- Spanwise distribution of heat transfer at station  $x/c \approx 0.950$  for angles of attack of  $20^\circ$ ,  $30^\circ$ , and  $40^\circ$ .  $\delta_e = 30^\circ$ .



(b)  $R_c = 0.77 \times 10^6$ .

Figure 12.- Continued.



(c)  $R_c = 2.70 \times 10^6$ .

Figure 12.- Concluded.

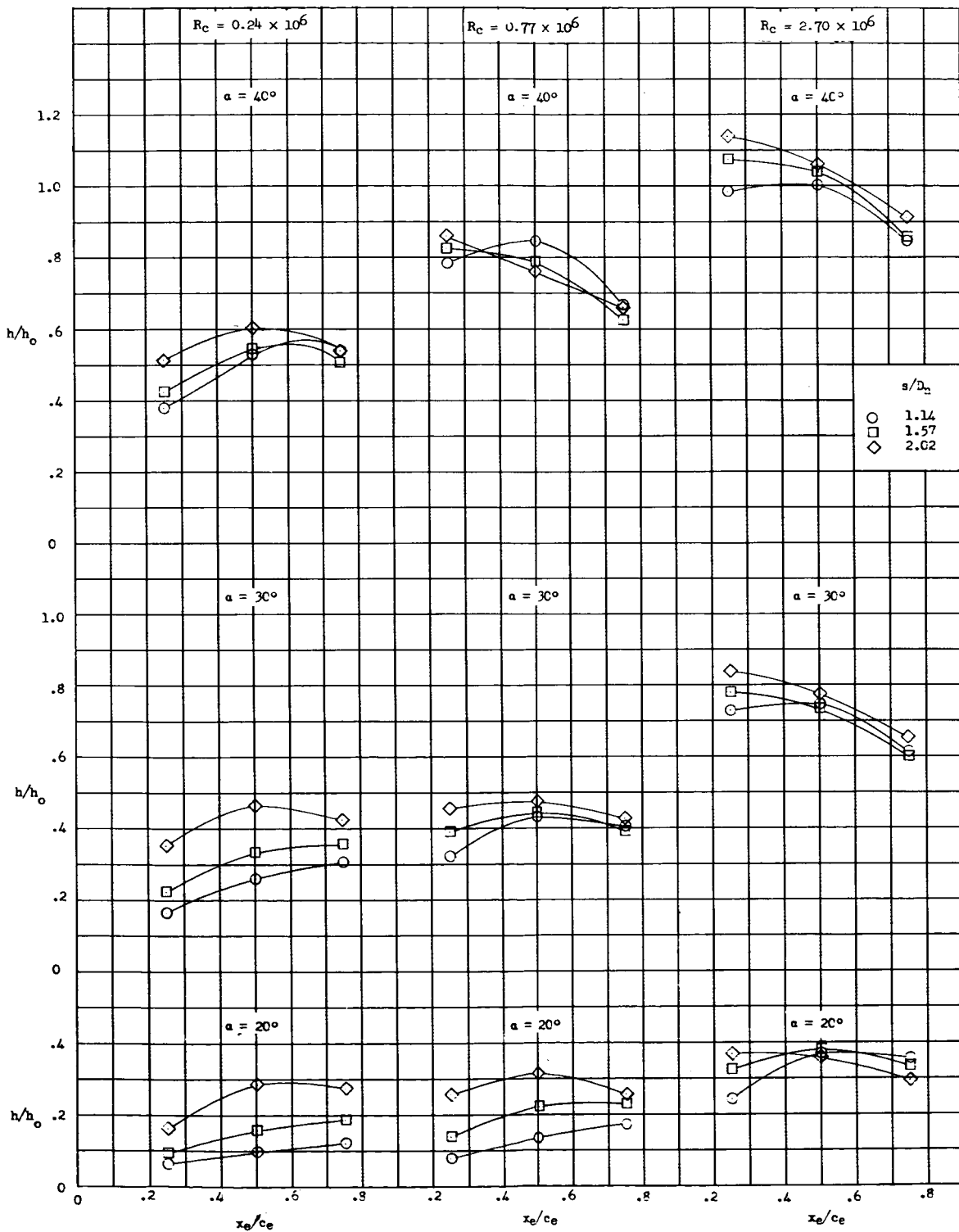


Figure 13.- Chordwise distribution of heat-transfer ratio on elevon.  $\delta_e = 30^\circ$ .

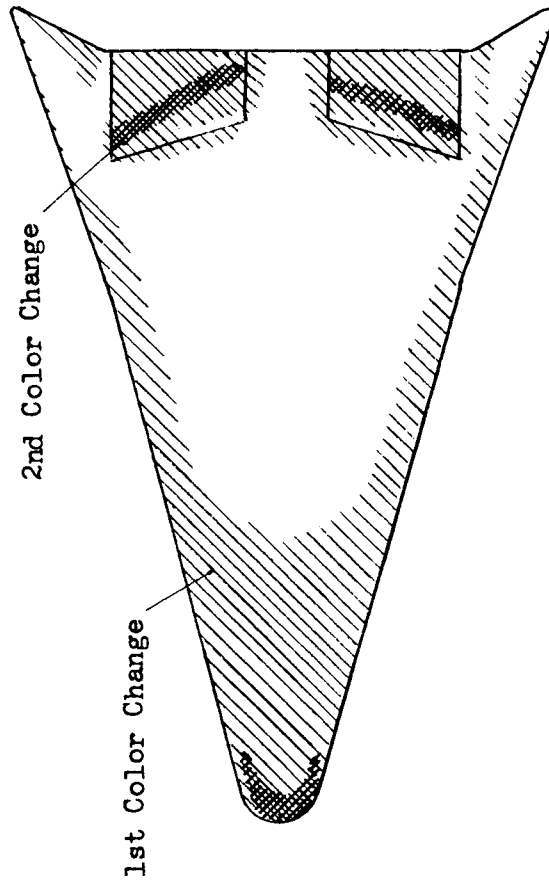
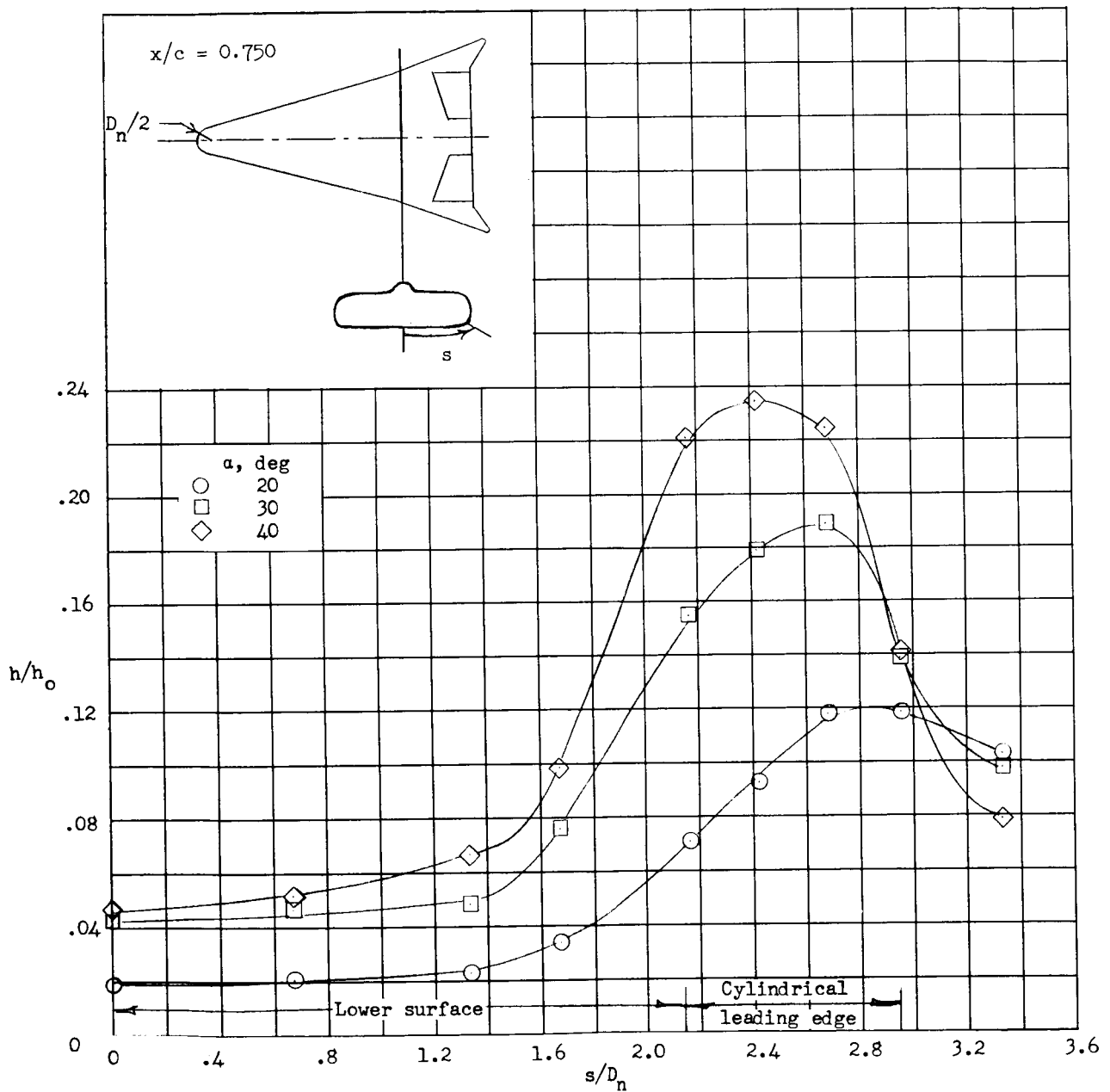
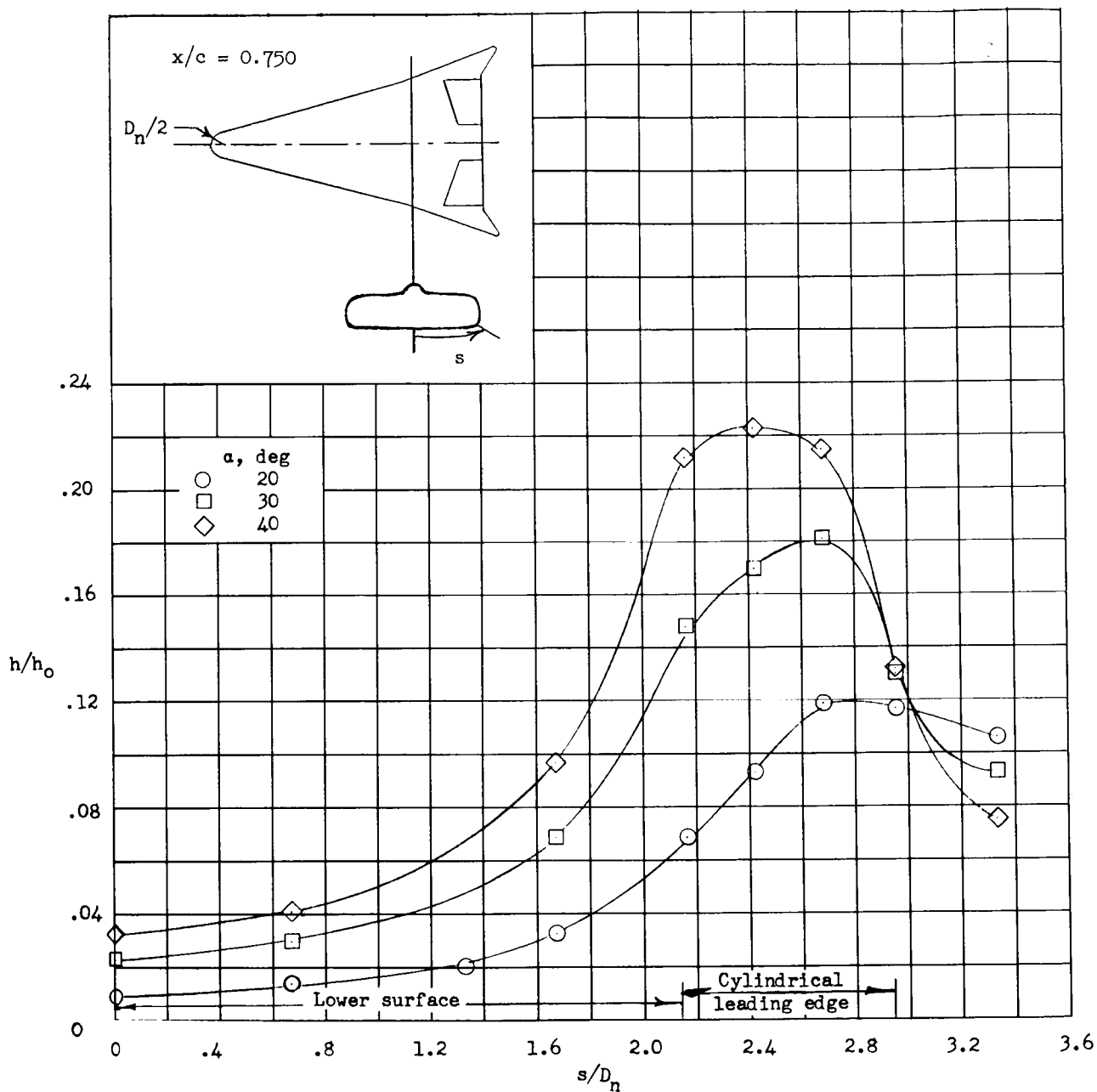


Figure 14.- Sketch of color changes of painted fiber-glass model tested at  $\alpha \approx 40^\circ$ ,  $\delta_e = 30^\circ$ , and  $R_c = 0.60 \times 10^6$ .



(a)  $Re = 0.24 \times 10^6$ .

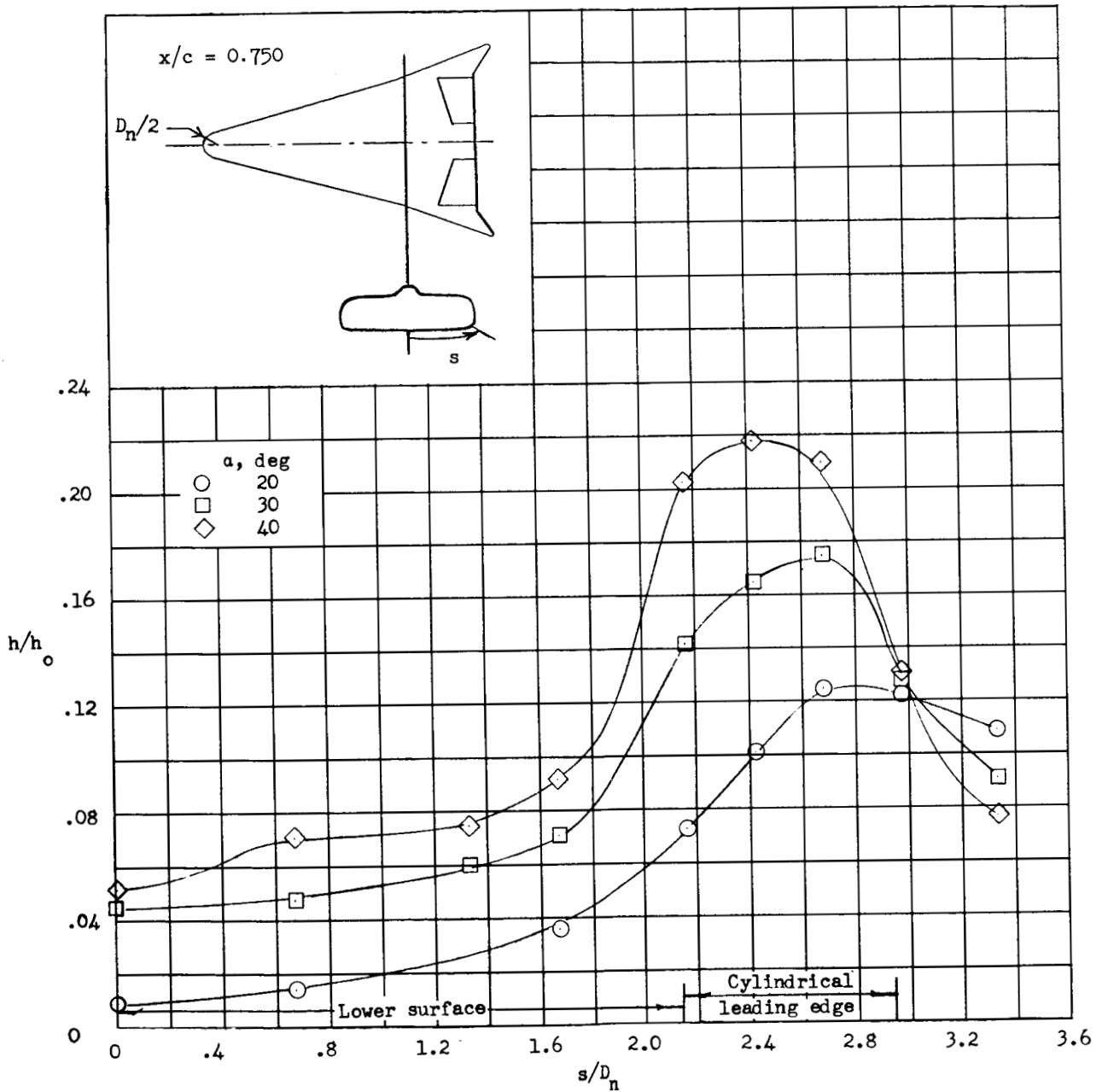
Figure 15.- Spanwise distribution of heat transfer at station  $x/c = 0.750$  for angles of attack of  $20^\circ$ ,  $30^\circ$ , and  $40^\circ$ .  $\delta_e = 30^\circ$ .



(b)  $R_c = 0.77 \times 10^6$ .

Figure 15.- Continued.

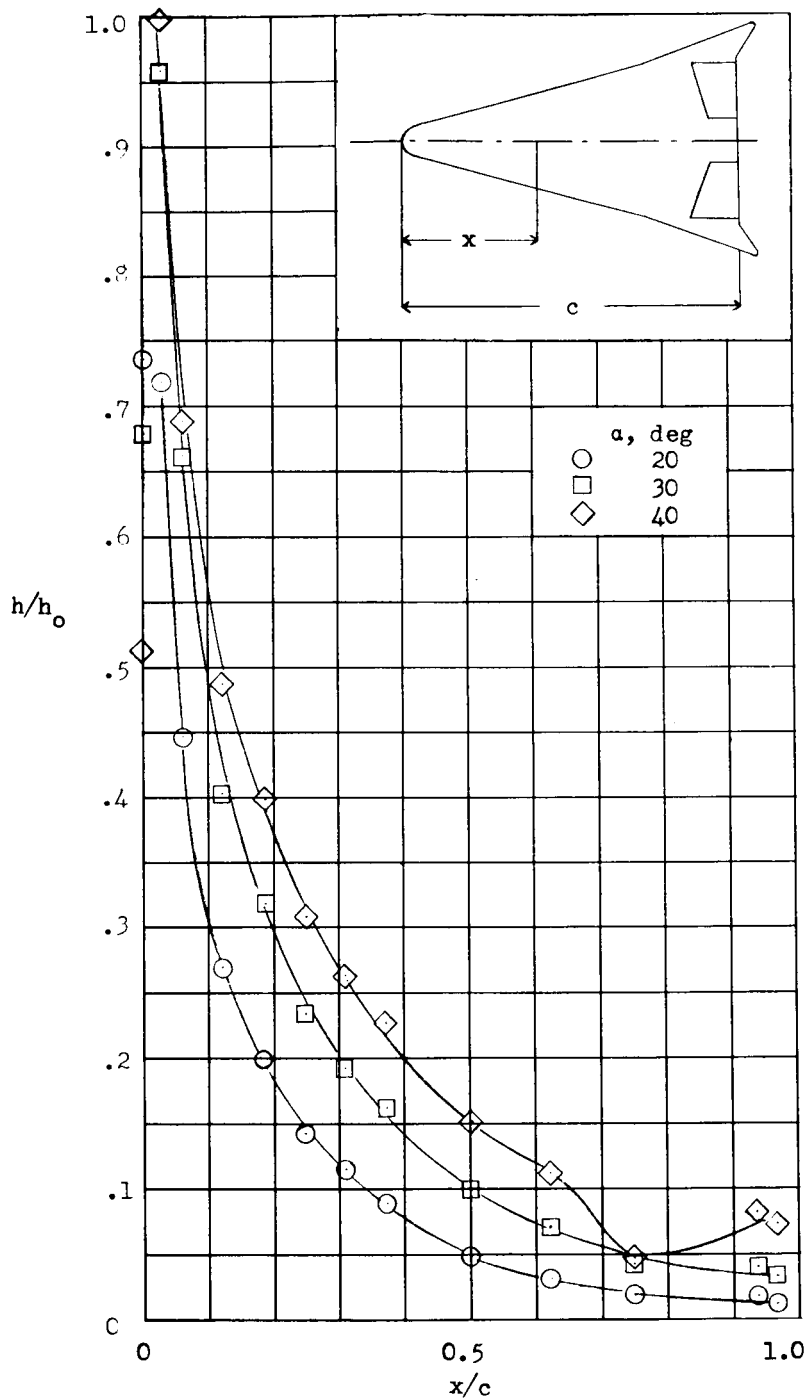
UNCLASSIFIED



(c)  $R_c = 2.70 \times 10^6$ .

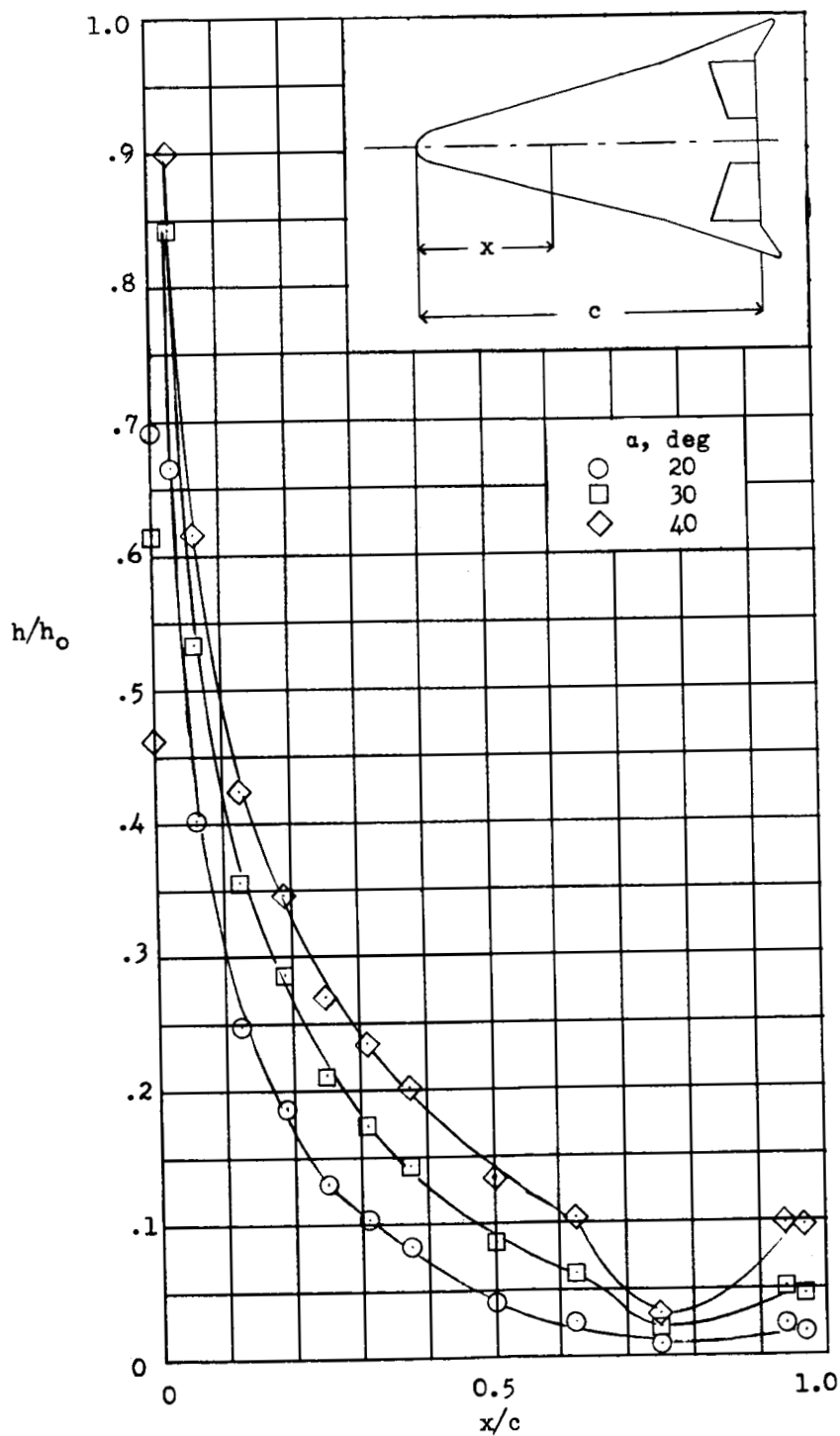
Figure 15.- Concluded.

UNCLASSIFIED



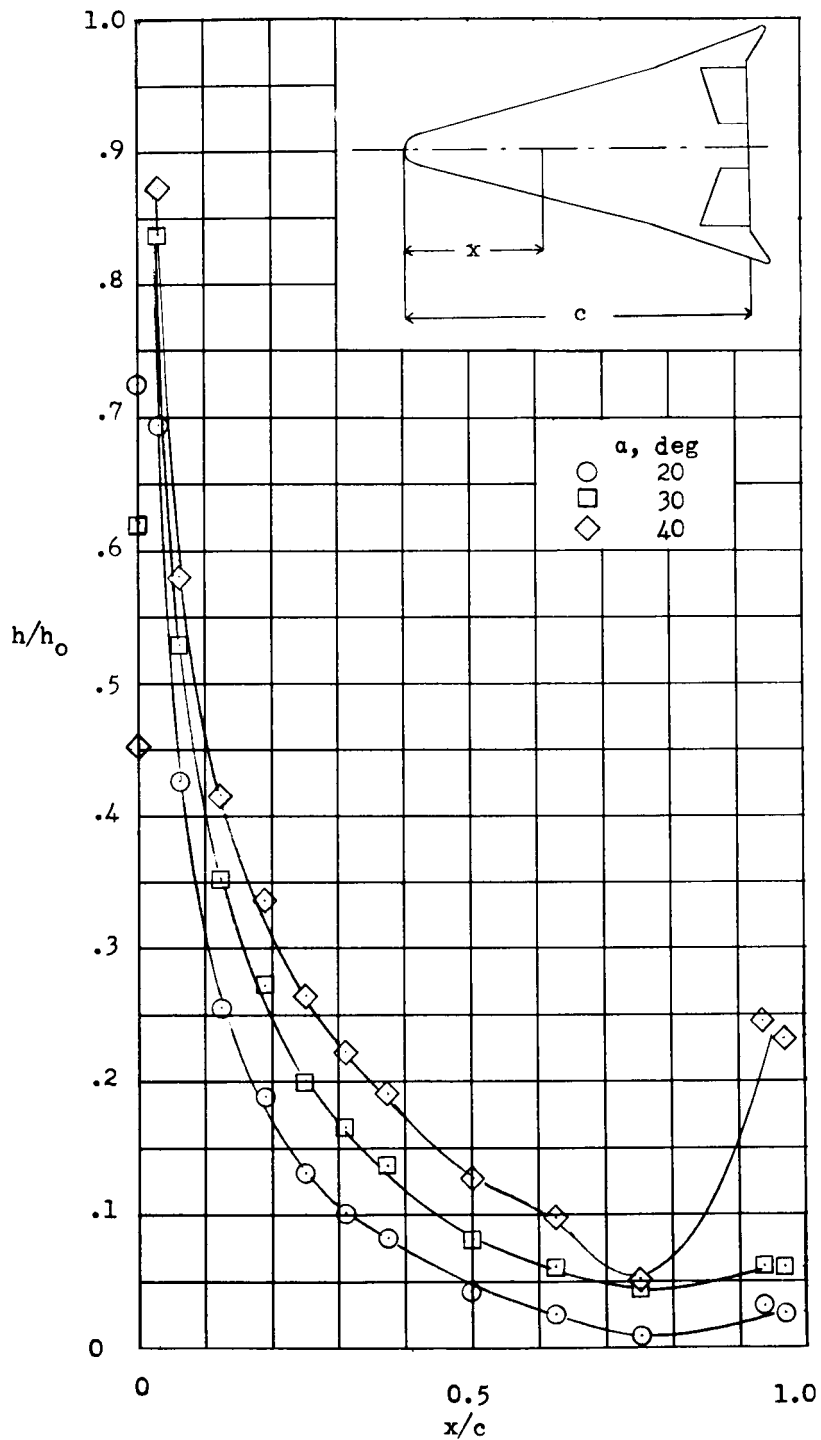
(a)  $Re = 0.24 \times 10^6$ .

Figure 16.- Center-line distributions of heat transfer at angles of attack of  $20^\circ$ ,  $30^\circ$ , and  $40^\circ$  with elevon deflected  $30^\circ$ .



(b)  $R_c = 0.77 \times 10^6$ .

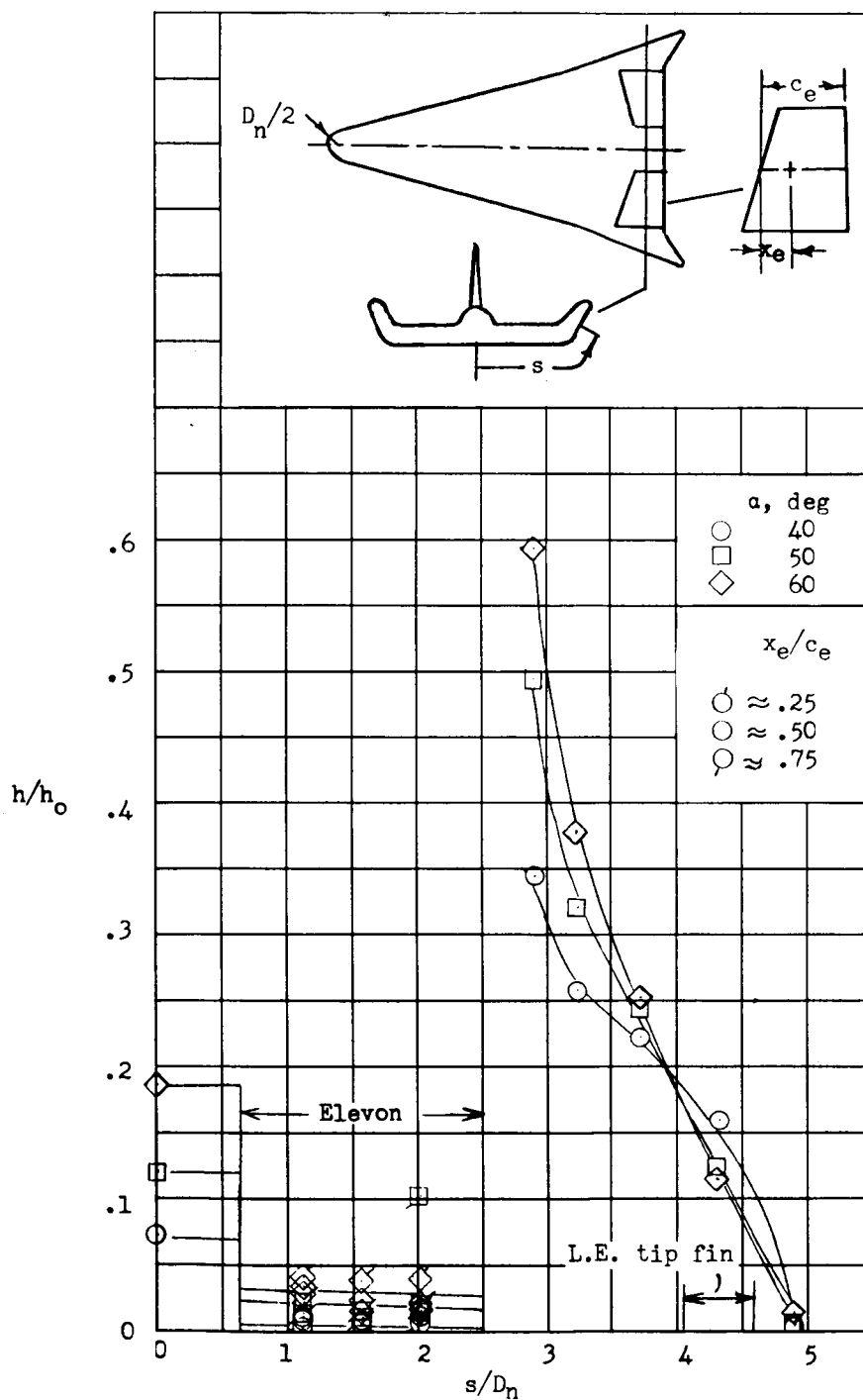
Figure 16.- Continued.



(c)  $R_c = 2.70 \times 10^6$ .

Figure 16.- Concluded.

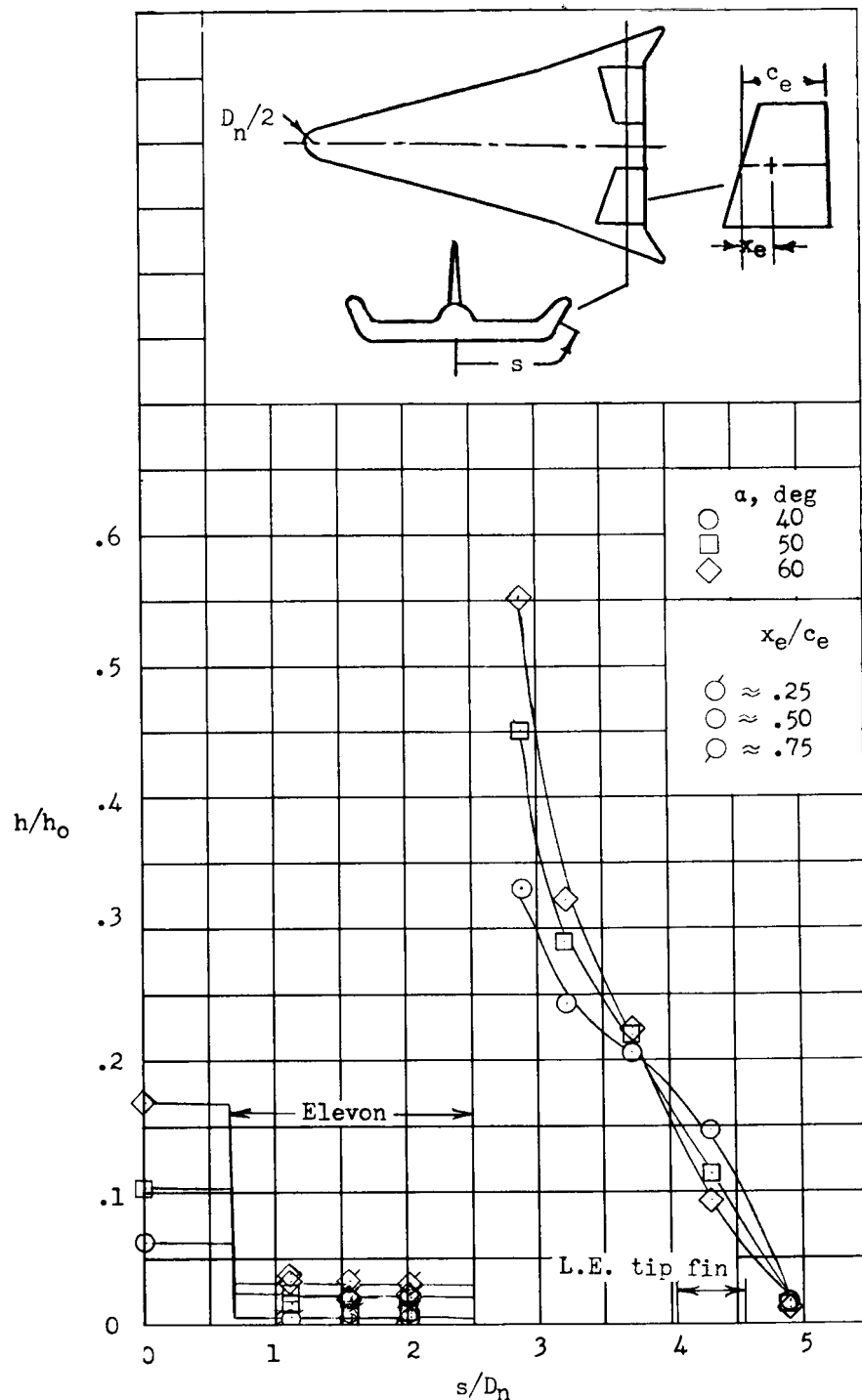
UNCLASSIFIED



(a)  $R_c = 0.24 \times 10^6$ .

Figure 17.- Spanwise distribution of heat transfer at station  $x/c \approx 0.950$  for angles of attack of  $40^\circ$ ,  $50^\circ$ , and  $60^\circ$ .  $\delta_e = -60^\circ$ .

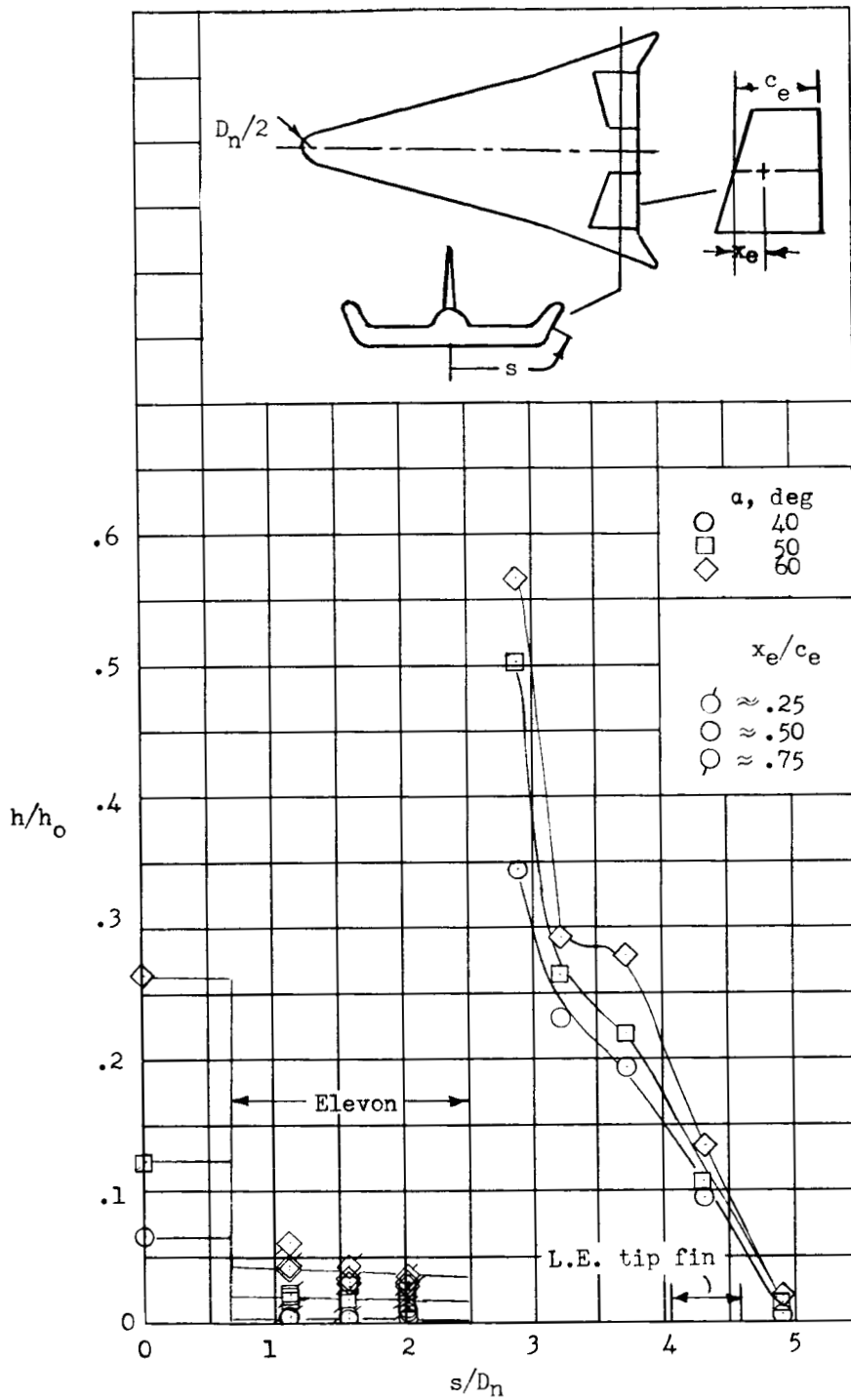
UNCLASSIFIED



(b)  $R_c = 0.77 \times 10^6$ .

Figure 17.- Continued.

UNCLASSIFIED



(c)  $R_c = 2.70 \times 10^6$ .

Figure 17.- Concluded.

CONFIDENTIAL

UNCLASSIFIED

UNCLASSIFIED

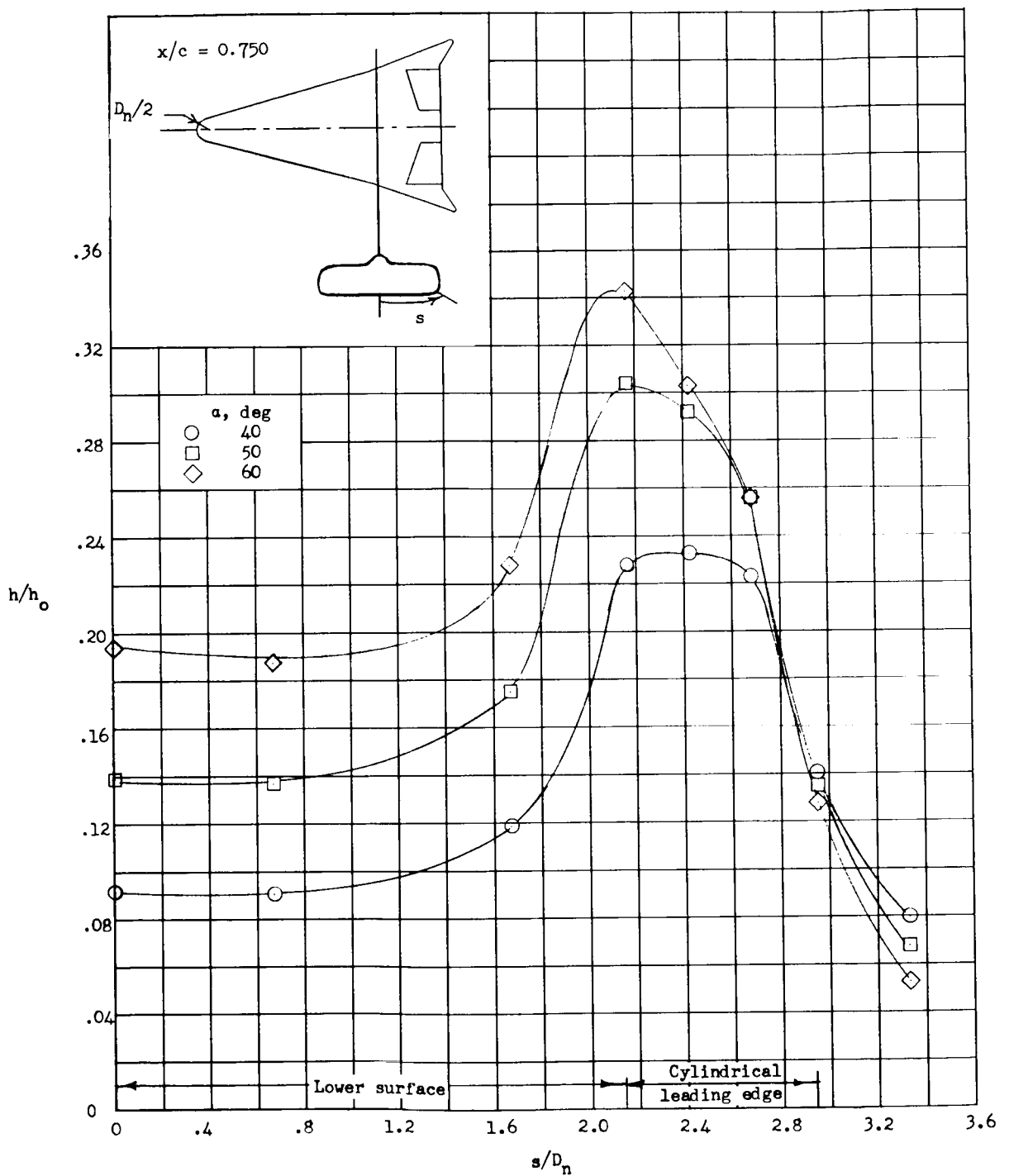
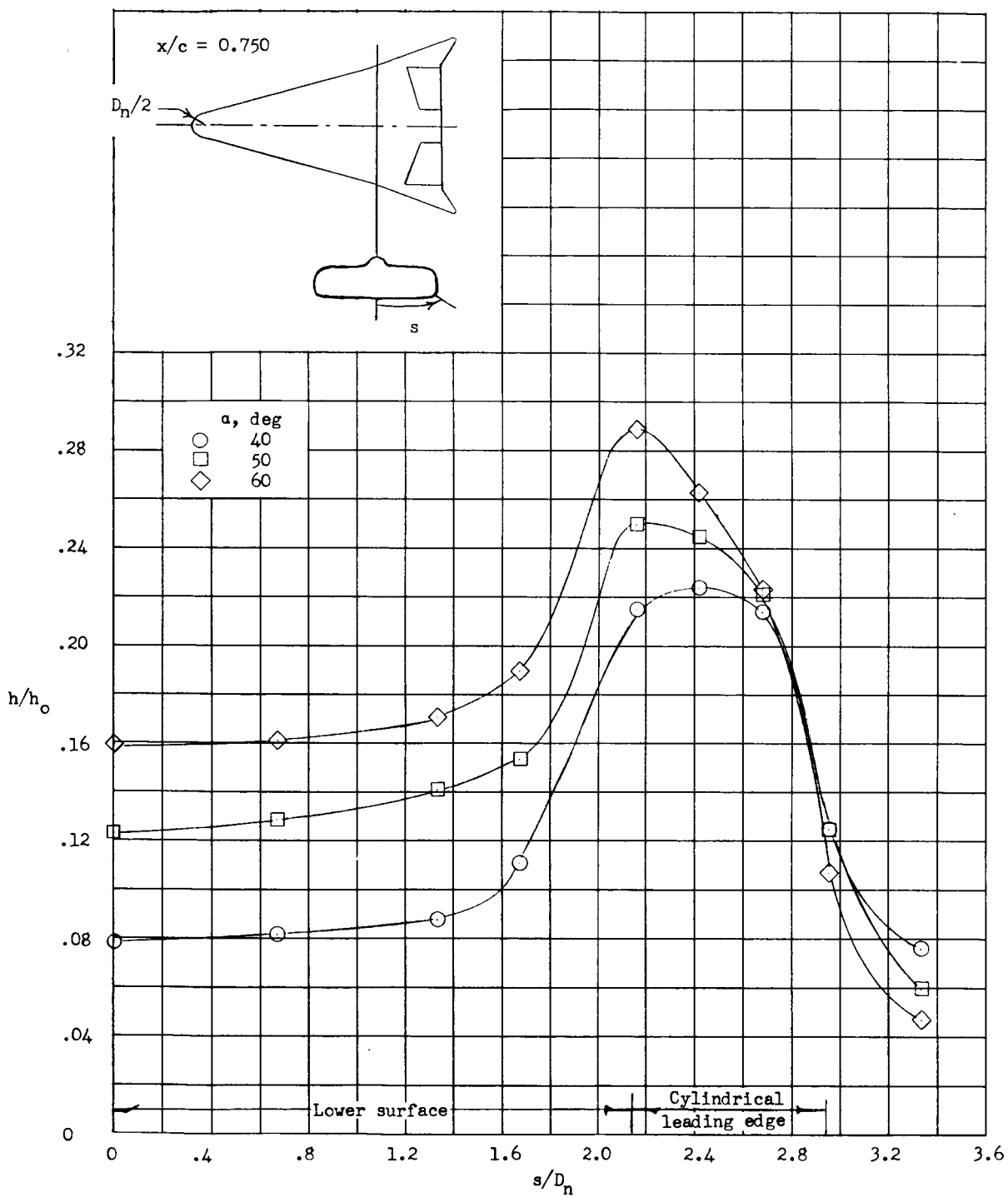
~~CONFIDENTIAL~~(a)  $R_c = 0.24 \times 10^6$ .

Figure 18.- Spanwise distribution of heat transfer at station  $x/c = 0.750$  for angles of attack of  $40^\circ$ ,  $50^\circ$ , and  $60^\circ$ .  $\delta_e = -60^\circ$ .

~~CONFIDENTIAL~~

UNCLASSIFIED



(b)  $R_c = 0.77 \times 10^6$ .

Figure 18.- Continued.

UNCLASSIFIED

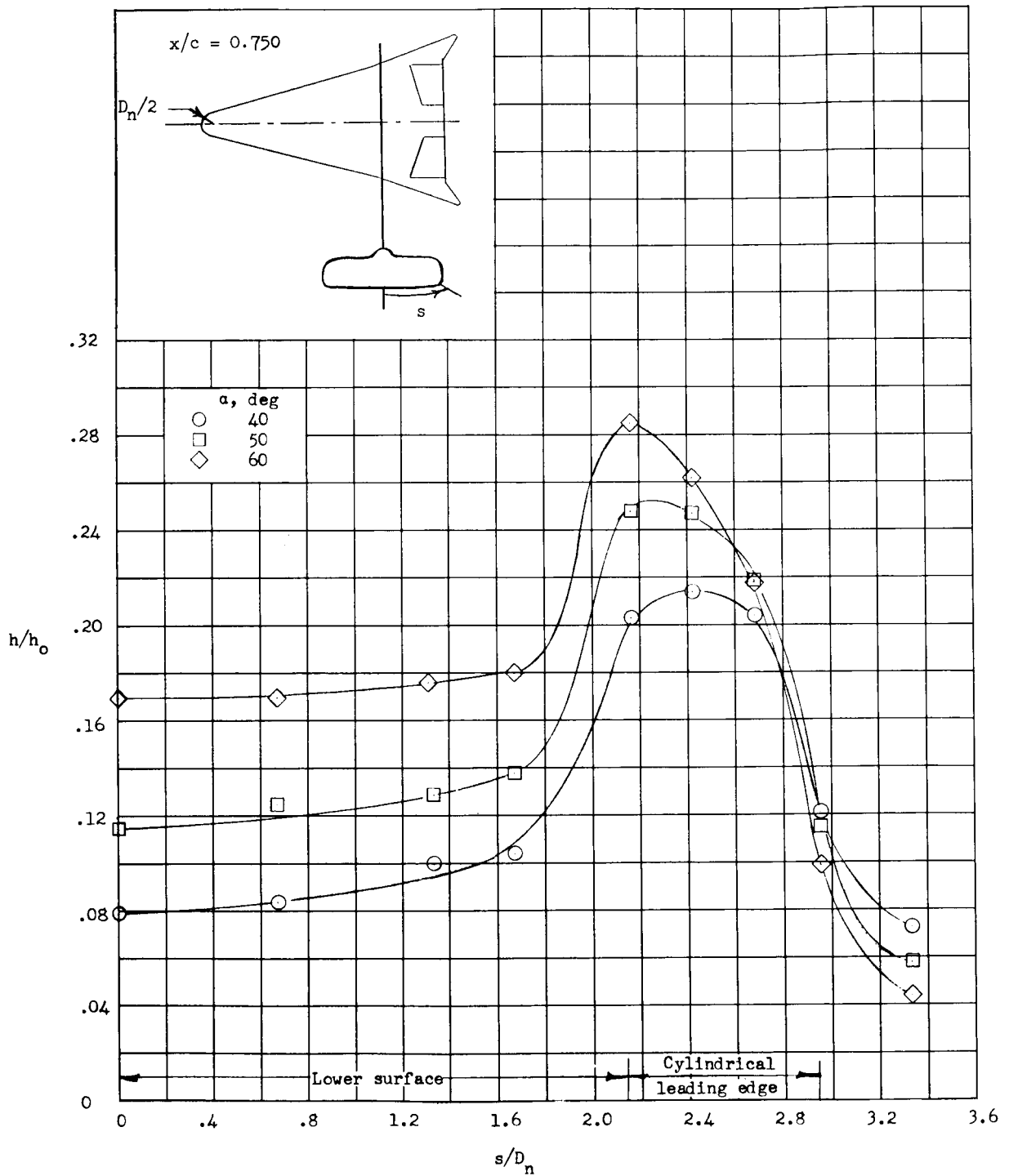
~~CONFIDENTIAL~~(c)  $R_c = 2.70 \times 10^6$ .

Figure 18.- Concluded.

UNCLASSIFIED

~~CONFIDENTIAL~~

~~CONFIDENTIAL~~

UNCLASSIFIED

*"The aeronautical and space activities of the United States shall be conducted so as to contribute . . . to the expansion of human knowledge of phenomena in the atmosphere and space. The Administration shall provide for the widest practicable and appropriate dissemination of information concerning its activities and the results thereof."*

—NATIONAL AERONAUTICS AND SPACE ACT OF 1958

## NASA SCIENTIFIC AND TECHNICAL PUBLICATIONS

**TECHNICAL REPORTS:** Scientific and technical information considered important, complete, and a lasting contribution to existing knowledge.

**TECHNICAL NOTES:** Information less broad in scope but nevertheless of importance as a contribution to existing knowledge.

**TECHNICAL MEMORANDUMS:** Information receiving limited distribution because of preliminary data, security classification, or other reasons.

**CONTRACTOR REPORTS:** Technical information generated in connection with a NASA contract or grant and released under NASA auspices.

**TECHNICAL TRANSLATIONS:** Information published in a foreign language considered to merit NASA distribution in English.

**TECHNICAL REPRINTS:** Information derived from NASA activities and initially published in the form of journal articles.

**SPECIAL PUBLICATIONS:** Information derived from or of value to NASA activities but not necessarily reporting the results of individual NASA-programmed scientific efforts. Publications include conference proceedings, monographs, data compilations, handbooks, sourcebooks, and special bibliographies.

*Details on the availability of these publications may be obtained from:*

SCIENTIFIC AND TECHNICAL INFORMATION DIVISION  
NATIONAL AERONAUTICS AND SPACE ADMINISTRATION

Washington, D.C. 20546

UNCLASSIFIED

~~CONFIDENTIAL~~